UNITED NATIONS UNIVERSITY
GEOTHERMAL TRAINING PROGRAMME
Orkustofnun, Grensasvegur 9,
IS-108 Reykjavik, Iceland

Reports 2012
Number 12

AQUIFER FLUID COMPOSITIONS AT THE BERLÍN GEOTHERMAL FIELD, EL SALVADOR IN 2012

Carlos Baltazar Hernandez Murga
LaGeo S.A. de C.V.
15 Avenida Sur, Colonia Utila
Nueva San Salvador, La Libertad
EL SALVADOR C.A.
bhernandez@lageo.com.sv

ABSTRACT

The Berlín geothermal reservoir is liquid-dominated and sub-boiling at deep levels with a temperature of ~300°C. However, after 20 years of continuous power production and the increase in power generation from 8 to109 MW, there has been a decline in pressure of about 20 bar with the result that extensive boiling of the aquifer water now occurs in the feed zone of some wells. This change in conditions affects scale formation potential from the boiling geothermal water.

Electric power generation from geothermal resources is important for El Salvador since it provides about 24% of the country's demands. Therefore, maintenance of the productive capacity and adequate resource management at Berlín are important variables for the company operating the field, LaGeo S.A. de C.V.

To quantify the scaling potential, it is necessary to understand the geochemical processes occurring in the reservoir, as well as changes in the chemical composition of the fluid as it boils in producing aquifers and wells, to lay out an appropriate exploitation and management plan and an adequate monitoring plan to help make timely and correct solutions concerning scaling problems that may occur in wells. In this study, an evaluation of the physical conditions of 11 production wells operating in the Berlín geothermal field was carried out. Ten wells with two-phase production were evaluated, supported by the WATCH program developed by Arnórsson et al. (1982), version 2.4 (Bjarnason, 1994), to calculate aquifer water compositions and aqueous species distribution for each well at selected aquifer temperatures. Temperature equations were used for equilibrium constants for selected mineral dissolution reactions, presented by Karingithi et al. (2010), to calculate the saturation indices for common hydrothermal minerals in geothermal reservoirs. These minerals include calcite, clinozoisite, epidote, grossular, magnetite, prehnite, pyrite, pyrrhotite and wollastonite.

1. INTRODUCTION

The Berlín geothermal field in El Salvador was developed for electric power generation. Presently, the installed capacity is 109 MWe. To date, a total of 38 wells have been drilled. Much data have been collected on well characteristics during the course of development and utilization of the field, including

lithology, hydrothermal alteration, downhole temperature and pressure, fluid and well discharge chemistry and enthalpy.

The present report uses all these data. Yet, the main focus is on modelling the aquifer fluid composition followed by an assessment of the state of the mineral-solution equilibria in producing feed zones. The results of this study form a basis for improved understanding of the deposition of some sulphide minerals in wellbores and surface equipment that is presently a concern for successful field operations.

2. BERLÍN GEOTHERMAL FIELD

2.1 Geology

El Salvador is a country located on the southern coast of Central America. The volcanic chain in this region is related to a tectonic subduction zone between the Cocos and Caribbean plates. Another important tectonic feature of the area is the boundary of the Caribbean plate with the North-American plate near Guatemala, as it defines the Motagua-Polochic fault system. Parallel to the Pacific coast of Central America, from Guatemala to Nicaragua, a graben formed that crosses El Salvador from West to East (Molnar and Sykes, 1969). A chain of volcanoes follows the southern margin of this graben. Figure 1 shows the tectonic map of Central America and the principal structures.

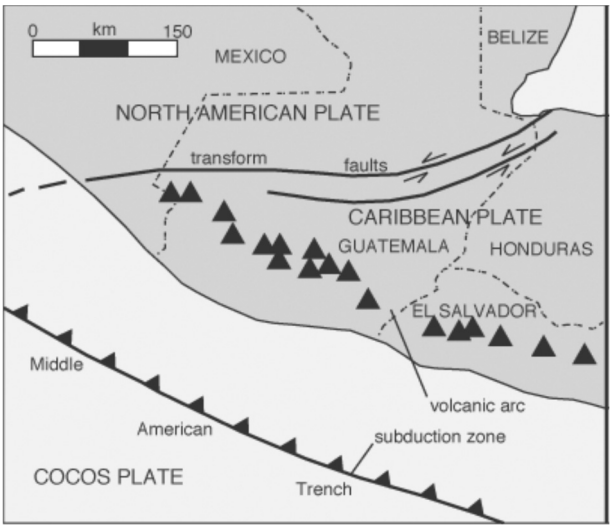

FIGURE 1: Simplified tectonic map of El Salvador

2.2 History of the development and production of the Berlín geothermal field

The Berlín geothermal field is located in the eastern part of El Salvador, 110 km from San Salvador, in the north-northwest running zone of the Tecapa Berlín volcanic complex within a NNW-SSE trending graben structure.

The Servicio Geológico Nacional of El Salvador undertook geoscientific studies of the geothermal area at Berlín in 1953. Interest in the geothermal potential of the area increased in the 1960s, when the Comisión Ejecutiva Hidroeléctrica del Río Lempa (CEL), the National Electricity Company, in co-operation with the United Nations Development Programme, undertook an exploratory survey that included drilling the first deep exploratory well, Tronador 1 (TR1), named after the principal fumarole in the Berlín Field, El Tronador. This first deep well was drilled in 1968. From 1978 to 1981, five additional wells were completed: TR2, TR3, TR4, TR5 and TR9. For political reasons, the project was halted, but in 1990 it was reactivated and its thermal potential was estimated to be 100 MWe (Electroconsult, 1993).

The Berlín geothermal field has been under exploitation for electric power generation since 1992 when two back pressure units were installed with a total capacity of 10 MWe. It was planned to use wells TR2 and TR9 as producers and TR1 as a reinjection well for the separated water. Due to the limited absorption capacity of well TR1, it was decided to put only one unit online, using well TR2 as a producer and well TR9 as a reinjection well for a short period of time (Montalvo and Axelsson, 2000).

From 1993 to 1995, three deep wells were drilled (TR8, TR10 and TR14) for reinjection purposes, and the second backpressure unit was put online in February 1995 with wells TR2 and TR9 as producers. The separated water was injected into wells TR1, TR8, TR10 and TR14. In 1999, two 28 MWe condensing type units were commissioned and, at the same time, the two backpressure units were decommissioned.

From 2003 to 2006, ten wells were drilled (TR14A, TR17, TR17A, TR17B, TR18, TR18A, TR19, TR19A, TR19B and TR19C). Of these, wells TR17 and TR18 were used for production and wells TR14A and TR19 for injection of spent brine. Figure 2 shows the Berlín geothermal field and the well and power plant locations.

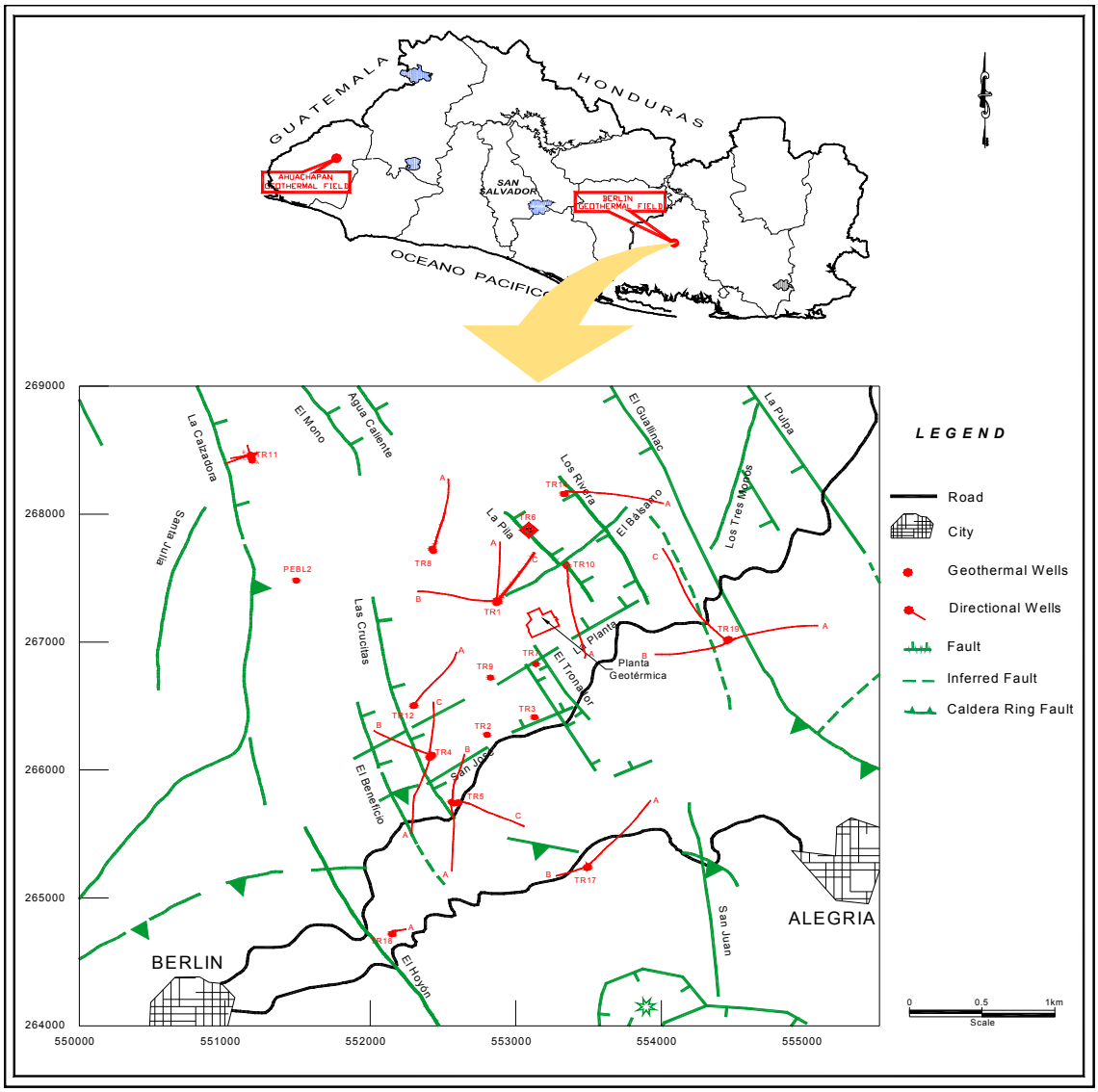

FIGURE 2: Berlín geothermal field and location of wells

In 2007, a 44 MWe condensing type unit and 9.2 MWe binary units were commissioned. At present, the total installed capacity is 109.2 MWe. Thirty eight wells have been drilled in the Berlín field; 16 wells are being used as producers and 18 for injection.

After 20 years of exploitation (1992-2012), the Berlín geothermal field is still a liquid-dominated system with temperatures in the range of 260-300°C according to measured temperatures in the production wells. The discharge enthalpy of production wells is usually 1100-1300 kJ/kg which corresponds to

liquid enthalpy at the temperature of producing aquifers. Only one well has high enthalpy and discharges dry steam. The steam fraction, at 11.5 bar separation pressure, in the wells connected to Units I and II is between 20 and 22%. The separation pressure of the wells connected to Unit III is 8.5-9.3 bar.

The production wells in the Berlín geothermal field were drilled to depths of 1000-2600 m, and the injection wells to depths of 500-3445 m. The elevation of the Berlín geothermal field ranges between 445 m a.s.l. in the reinjection zone (well TR11), and 1080 m a.s.l. in the production zone wells TR17 (Rodriguez and Monterrosa, 2011).

2.3 Conceptual model for the Berlín geothermal field

The heat source feeding the geothermal system is considered to be related to the magma chamber below the Berlín caldera, i.e. the more recent post-caldera magma chamber (Figure 3). The heat source is located under the Berlín-Tecapa volcanic complex. The recharge to the system is meteoric water, as indicated by isotope data, and is thought to be concentrated along the highly fractured tectonic structures. The circular caldera faults which act as hydrological barriers, limit the recharge of meteoric water from within the caldera. The main upflow occurs in the southern part of the caldera and the hot fluid flows north along the graben structures.

The rocks found in the area of the geothermal field are mainly andesitic lava flows with interbedded tuffs. The tuffs are thick at deep levels (1883-1943 m) in the central part of the caldera where they range in composition from basaltic to silicic. Near the surface the tuff layers are thinner. At depth, the reservoir rock contains mainly the following alteration minerals: quartz, calcite, chlorite and penninite, wairakite, epidote, illite, albite and ferric oxides (CEL, 1999).

Table 1 summarizes the general lithology identified within Berlín geothermal field (see also Figure 3), and Tables 2-4 that provide information on the mineralogy encountered by drilling into the different zones in the field.

TABLE 1: General stratigraphy of the Berlín geothermal field

Unit	Lithology	Characteristics	Thickness (m)
I	Andesite to basaltic andesite	Recent deposits	600-800
II	Ignimbrite intercalated with scoria and thin layers of andesite	Intermediate aquifer	570-850
III	Fine silicified lithic tuff	Cap rock	100-345
IV	Andesite to basaltic andesite with lithic tuff and some dykes and intrusions of diorites	Reservoir	370-920

TABLE 2: Mineralogy in the northern part of Berlín

Facies	Key Minerals	Depth (m)	Temp (ºC)
Argillic	Cri, Heul, Mon, Sp	0-369	50-100
Argillic-Phyllic	Cor, + Sp, + Heul, << Cri	369-690	100-150
Phyllic	Cl, Qz, Lau, Ill-Mon, + Wai, + Cor	690-1320	150-220
Phyllic-Propylitic	Ill, Chl (well–developed), >> Qz, Wai, + Ep	1320-1650	220-250
Propylitic	Ep, + Wai, < Cal, + Crd	1650- final depth	>250

Anh: anhydrite; Cal: calcite; Cor: corrensite; Crd: cordierite; Cris: cristobalite; Chl: chlorite; Clinop: clinoptilolite; Ep: epidote; Epis: epistilbite; Heul: heulandite; Ill: illite; Illite-mont: illite-montmorillonite; Lau: laumontite; Mon: montmorillonite; Ox: iron oxides, Pen: penninte; Preh: prehnite; Qz: quartz; Sp: saponite; Si: quartz, Cl/Sm: corrensite, Wai: wairakite; <: rare; <<: very rare, >>: very abundant, ±: sometimes present, sometimes absent.

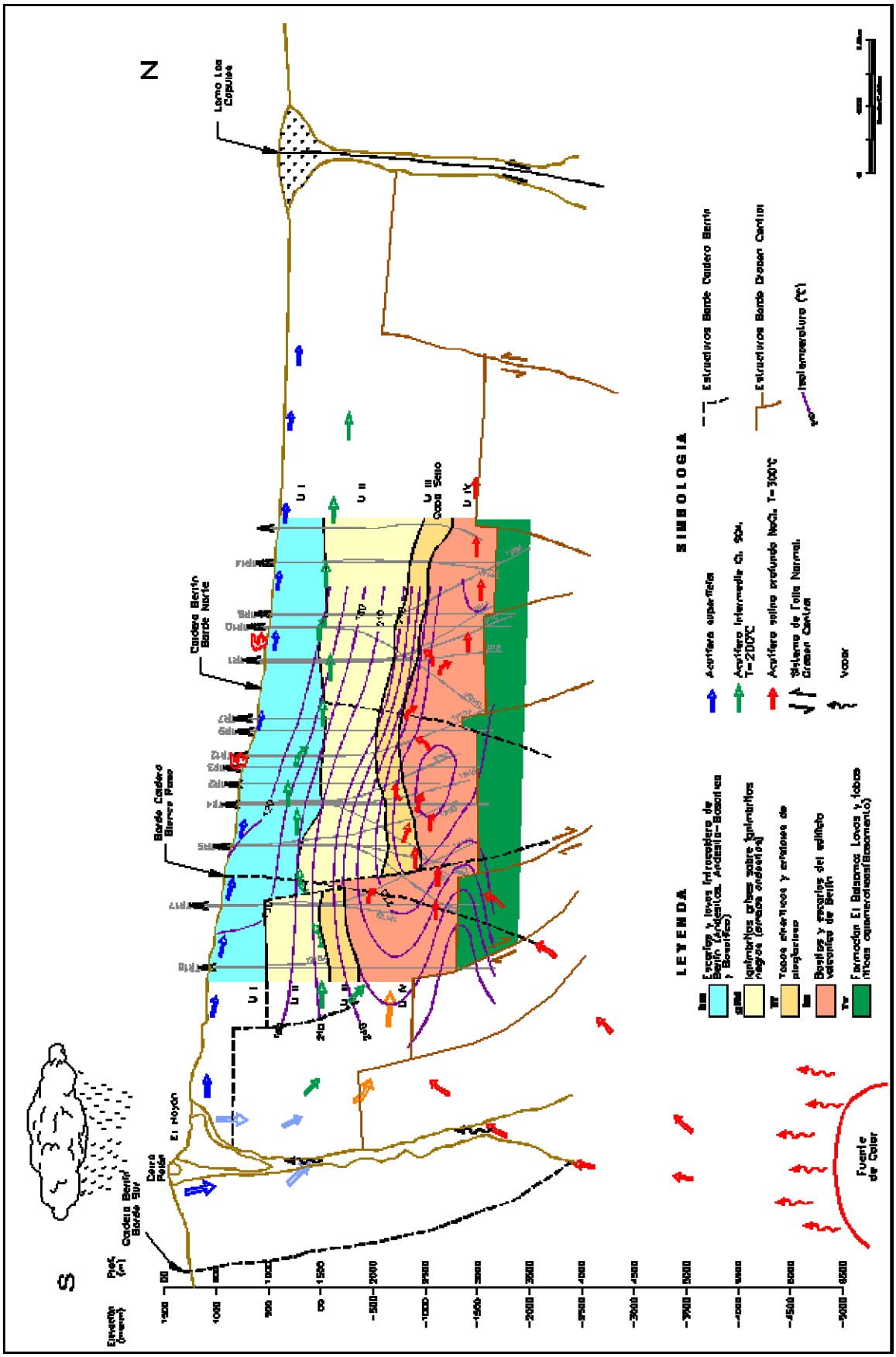

FIGURE 3: Berlín conceptual model

TABLE 3: Mineralogy in the central part of Berlín

Facies	Key Minerals	Depth (m)	Temp. (ºC)
Argillic	Cri, Heul, Mon, Sp	0-390	50-100
Argillic-Phyllic	Cor, + Sp, + Heul, << Cri	390-694	100-150
Phyllic	Chl, Qz, Lau, Ill-Mon, + Wai, +Cor	694-1517	150-220
Phyllic-Propylitic	Ill, Chl (well–developed), >>Qz, Wai, + Epi	1517-1700	220-250
Propylitic	Ep, + Wai, <Cal, + Crd	1700-2500	>250

See Table 2 for abbreviation of mineral names

TABLE 4: Mineralogy in the southern part of Berlín

Facies	Key minerals	Depth (m)	Temp (°C)
Argillic	Cl/Sm, Ox, <Ca, Si, <<Qz, < Heul, Clinop, Epis	0-370	50-120
Argillic-Phyllic	Cl/Sm, Ox, Ca, <Chl, < Qz	370 – 700	120-180
Phyllic	Ca, Chl, <Pen, Qz <Ep, Preh, Anh, <Wai	700 – 1200	180-220
Phyllic-Propylitic	Ca, Chl, Pen, Qz, Wai, Ep, Preh, Ilite	1200 – 1550	220-260
Propylitic	Chl, Pen, <Cal, Wai, >> Ep	1550 – 2600	>260

See Table 2 for abbreviation of mineral names

Based on chemical data, three types of aquifers have been identified in the Berlín geothermal field: (1) a low-salinity aquifer with 1,600 ppm Cl at a depth between 200 and 300 m a.s.l.; (2) an intermediate salinity aquifer with fluid salinity of 6,600 ppm Cl at around sea level; and (3) a deeper saline aquifer with fluid having 8,000-12,000 ppm Cl at a depth ranging from -800 to -1,200 m a.s.l. (Santos, 1995).

The water discharged from the Berlín reservoir is of the sodium-chloride type with a chloride content ranging from 3,000 to 7,000 ppm, pH values between 6.1 and 7.5 and TDS between 7,000 and 20,000 ppm. The gas/steam ratio is usually 0.1-0.3% in steam at ~12 bar-a separation pressure.

3. SAMPLING AND ANALYSIS

3.1 Sample collection

Steam and water samples were collected at the wellhead of production wells using either a Webre separator or sampling ports installed at a cyclone separator. Steam samples were collected in duplicate into evacuated gas sampling bulbs containing 50 ml of 4M NaOH solution. Water samples were collected at the same pressure as steam samples and filtered through 0.2 µm cellulose acetate membrane filters into high density polyethylene bottles using a filter holder of the same material. Each sample was split into two portions, 250 ml each; one of them was preserved, adding 2.5 ml of supra pure concentrated HNO_3 for the analysis of major cations (Na, K, Ca, and Mg), boron and silica; the second portion was used for pH, chloride, total carbonate carbon, sulphide and sulphate analysis (Melara, 2011). Table 5 lists the status of production wells in Berlín.

3.2 Analysis

Table 6 lists the analytical methods used for the analysis of the steam and water samples by LaGeo Geochemistry Laboratory.

TABLE 5: Production wells in Berlín geothermal field

No.	Name	Status	Condition - deviation	Elevation (m a.s.l.)	Start drilling	End drilling	Depth (m)
1	TR1	R/A	VERT	552	22-Jun-68	20-Jul-68	1458
2	TR1A	R	N-05-E	573	24-Apr-98	27-nov-98	2330
3	TR1B	R	N-72-W	573	12-May-98	26-Jan-99	2432
4	TR1C	R	N-38-E	573	27-Jan-99	21-Apr-99	2495
5	TR2	P	VERT	752	14-Jan-78	02-Jun-78	1903
6	TR3	R/P	VERT	760	24-Apr-79	30-Oct-79	2300
7	TR4	P	VERT	767	23-Jan-80	08-Jul-80	2379
8	TR4A	R/P	S-04-W	767	11-May-97	04-Dec-97	2157
9	TR4B	P	N-56-W	767	09-Dec-97	30-Mar-98	2292
10	TR4C	P	N-05-W	767	02-Apr-98	24-Aug-98	2179
11	TR5	P	VERT	853	30-Jan-81	04-Jul-81	2086
12	TR5A	P	S-03-W	840	02-Feb-98	29-Aug-98	2325
13	TR5B	P	N-17-E	840	02-Mar-98	31-Dec-98	2097
14	TR5C	P	S-70-E	840	16-Mar-98	23-Mar-99	2343
15	TR6	A	n.a	n.a	n.a	n.a	n.a
16	TR7	R	VERT	657	01-Sep-99	04-Oct-99	750
17	TR8	R	VERT	466	17-Mar-94	31-May-94	2323
18	TR8A	R	N-17-E	466	10-Jan-99	26-May-99	2590
19	TR9	P	VERT	649	04-Sep-80	28-Dec-80	2298
20	TR10	R	VERT	537	02-Feb-95	05-Apr-95	2333
21	TR10A	R	S-05-E	537	30-May-02	24-Sep-02	2326
22	TR11ST	R	VERT	445	12-Jun-97	27-Nov-97	2044
23	TR11A	R	VERT	445	04-Dec-97	14-Jan-98	503
24	TR11B	R/A	N-10-W	445	17-Jan-98	11-Feb-98	614
25	TR11C	R/A	S-70-W	445	15-Feb-98	29-Mar-98	650
26	TR12	R	VERT	675	07-Jul-99	17-Aug-99	733
27	TR12A	R	N-40-E	675	10-Sep-98	04-Jul-99	2428
28	TR14S BIS	R	VERT	457	19-Dec-93	25-May-00	137
29	TR14A	R	S-75E	457	06-Dec-05	21-Feb-06	2336
30	TR17	P	VERT	1073	07-Jul-03	01-Dec-03	2600
31	TR17A	P	N-36-E	1073	04-Feb-04	22-Jun-04	2690
32	TR17B	P	S-74W	1073	01-Dec-04	03-Jan-05	n.a
33	TR18	P	VERT	995	18-Sep-03	25-Feb-04	2660
34	TR18A	P	N-77-E	995	05-May-04	30-Jul-04	1085
35	TR19	R	VERT	775	10-Jun-05	05-Aug-05	n.a
36	TR19A	R	N-89.78-E	775	09-Aug-05	30-Nov-05	2369
37	TR19B	R	S-75-W	775	05-Dec-05	31-Mar-06	3125
38	TR19C	R	N28.70-W	775	15-Apr-06	30-Oct-06	3455

P: Productor; R: Reinjector; A: Abandoned; n.a: Data not available

TABLE 6: Analytical methods used for steam and water samples

Steam sample		Water sample	
Analyte	**Method**	**Analyte**	**Method**
CO_2	Titration with HCl	Na	AAS
H_2S	Titration with sodium thiocyanate	K	AAS
He	GC with thermal conductivity detector	Ca	AAS
H_2	GC with thermal conductivity detector	Mg	AAS
N2	GC with mass detector	B	AAS
Ar	GC with mass detector	SiO_2	AAS
CH_4	GC with mass detector	Cl	Titration with $AgNO_3$
O_2	GC with mass detector	SO_4	UVS
		CO_2	Titration with HCl and NaOH
		pH	Potentiometric

GC = Gas Chromatography; AAS = Atomic Absorption Spectrophotometry; UV Spectrophotometer (Melara, 2011)

TABLE 7: Composition of water and steam samples collected from wells at Berlín.
Concentrations are in ppm for water samples (ppm or mg/kg) and in mmoles/kg for steam samples.

Sample site	Produc. casing shoe depth (m)	Sample date	Discharge enthalpy (kJ/kg)	Water collect. press. (bar-g)	Collect temp. (°C)	Water sample														Gas sample						
						CO_2[a]	H_2S	NH_3	B	SiO_2	Na	K	Mg	Ca	Cl	SO_4	Al[b]	Fe[b]	pH	CO_2	H_2S	NH_3	H_2	O_2	CH_4	N_2
TR4	1319	2004- 2012	1347	10	26	6.49	0.49	2.01	n.a	762	2858	583	0.103	48.4	5106	19.8	0.227	0.22	6.66	68	14.3	0.151	0.95	0.031	0.158	1.82
TR4B	1750	2098-2012	1336	9.8	40	15.55	2.05	0.25	91.8	755	2291	502	0.059	32.1	4151	14	0.334	0.037	7.05	113.7	12.4	0.063	1.47	0.028	0.179	2.77
TR4C	1508	1998-2012	1319	9.3	45	9.49	0.36*	0.26	117.1	722	3224	658	0.143	80.6	5834	17	0.182	0.028	6.76	105.6	11.4	0.064	1.26	0.024	0.204	3.47
TR5	1271	2004-2012	1279	10.7	39	2.56	0.87	0.24	115.3	792	3157	690	0.051	46.2	5696	12.1	0.231	0.048	6.3	58.5	13.3	0.046	0.83	0.016	0.164	1.26
TR5B	1600	1999-2012	1273	10.5	38	3.92	0.59	0.17	123.6	748	3569	726	0.071	90.1	6450	11	0.253	0.17	6.29	59.2	10.3	0.06	0.82	0.016	0.154	1.33
TR5C	1573	2000-2012	1279	11	46	3.2	0.31*	0.51	129	729	3740	734	0.148	126.7	6794	11.5	0.219	0.094	6.12	54.9	10.5	0.06	0.78	0.013	0.157	2.23
TR9	1277	1993-2012	1192	11	99	12	0.14*	0.44	127.2	677	3653	707	0.06	134	6585	12.8	0.313	0.029	6.88	71.1	9.1	0.115	0.89	0.011	0.161	1.22
TR17	1360	2008-2012	1172	8.2	90	2.49	0.19*	0.21	155.4	774	4445	812	0.174	190.1	8196	11.6	0.133	0.213	6.2	50.6	9	0.029	0.11	0.012	0.006	0.53
TR17A	1033	2007-2012	1172	7.8	60	3.29	0.7*	0.25	147.1	554	4188	682	0.278	250.5	7637	28.1	0.316	0.536	6.67	34.3	8.5	0.062	0.07	0.012	0.009	0.84
TR18	881.8	2006-2012	1181	8.5	67	15.84	1.17	0.35	86.2	627	1998	309	0.027	44.9	3441	26.8	0.325	0.12	7.47	79.9	12.3	0.123	0.13	0.017	0.013	1.86

a: Total carbon by titration; b: Data from the special analysis to wells samples is an average from the 2005 to 2011;
*: Data used are averaged from February and August 2012; n.a: not analysed.

3.3 Source of the analytical data

LaGeo has compiled numerous chemical analyses of well fluids from the Berlín geothermal field. For this report, representative analyses were selected from 10 of the following 16 producing wells: TR2, TR3, TR4, TR4A, TR4B, TR4C, TR5, TR5A, TR5B, TR5C, TR9, TR17, TR17A, TR17B, TR18, TR18A in the area that contained complete analyses of all major components and selected trace elements. The averages of individual component concentrations of the selected analyses are given in Table 7. Two production wells, TR4A and TR3, were earlier used as injection wells. As seen from Table 7, analytical data were not used from these wells for the present study.

The selection of the 10 wells was based on data necessary for the identification of the depth level of producing aquifers and their temperatures. The data include measurements of temperature and pressure downhole, and circulation losses during drilling in addition to components used as geothermometers.

4. PHYSICAL CHARACTERISTICS OF THE BERLÍN GEOTHERMAL FIELD

4.1 Temperature and pressure

The Berlín field is liquid-dominated and sub-boiling at deep levels, verified by temperature and pressure logging under thermally stabilized conditions. During discharge, the first depth-level of boiling in some of the wells is within the production casing, but in feed zones in others, as shown by pressure and temperature measurements carried out during discharge. The highest recorded temperature is 307°C (TR5B). One well discharges dry steam. It has a relatively shallow aquifer, 1000-1200 m deep, indicating the existence of a vapour cap on top of the liquid reservoir. This cap may have formed as a consequence of reservoir pressure drawdown by the exploitation of the field.

During drilling, *well TR4* had partial loss of circulation at 1865-1948 m depth and complete loss below 1948 m. Measured temperature, T, in this depth range was 284-286°C and pressure, P, ~116 bar indicating sub-boiling conditions (Figure 1, Appendix I). P and T did not change at this depth during discharge showing that the first depth level of boiling is at a higher level, or around 900 m. Quartz and Na-K geothermometer temperatures were 277 and 275°C, respectively (Table 8).

TABLE 8: Enthalpy and aquifer temperatures in selected wells at Berlín

Well	Circulation losses (m)	Meas. temp.[a] (°C)	T Qz[b] (°C)	T Na-K[c] (°C)	Selec. temp.[d] (°C)	Measure enthalpy[e] (kJ/kg)	Liq. enthalpy at sel. temp (kJ/kg)	Liq. enthal. diff. (kJ/kg)	Remarks
TR4	PL: 1865-1948 TL: 1948-2379	286	287	275	283	1347	1253	94	Boiling starts in well
TR4B	PL:1869-1892 TL: 1944-2292	294	285	289	289	1336	1285	51	Flashing in the formation
TR4C	PL: 1761-2179 TL: 1752	283	280	276	280	1319	1237	82	Flashing in the formation
TR5	PL: 1650-1830 TL: 1830-2086	305	290	297	297	1279	1328	-49	Flashing in the formation
TR5B	PL: 1671-2000 TL: 2000-2097	307	281	281	291	1273	1295	-22	Boiling starts in well
TR5C	PL: 1864-1996 TL: 1996-2343	294	283	271	283	1279	1253	26	Flashing in the formation
TR9	PL: 1448-1663 TL: 1663-2298	286	273	275	281	1192	1242	-50	Boiling starts in well
TR17	n.a	258	261	263	269	1172	1180	-8	Boiling starts in well
TR17A	PL: 1750-1820 TL: 2000-2690	286	237	250	263	1172	1150	22	Boiling starts in well
TR18	TL: 1875-2660	266	257	246	265	1181	1160	21	Boiling starts in well

a: Maximum temperature in wells as based on loggings;
b: Quartz equilibrium temperature using data on quartz solubility from Arnórsson (2000);
c: Na-K geothermometer temperatures based on Arnórsson et al. (2000) speciation program;
d: Select temperature for calculating aquifer water compositions using WATCH;
e: The discharge enthalpy was measured by recording critical lip pressure and measuring water flow rate (Russell James method). It tends to give high enthalpy values, by as much as 10%. The differences between measured and calculated fluid discharge enthalpy are not considered significant. Hence, all wells are assumed to have liquid enthalpy;
n.a: Data not available

In *well TR4B*, which is 2292 m deep, total loss of circulation during drilling occurred at 1900 m. Temperature at this depth was close to 300°C and the pressure was 120 bar (Figure 2 in Appendix I). The quartz and Na-K geothermometers indicated a feed zone temperature of 281°C which is reasonably close to the measured temperature at 1900 m, supporting the supposition that most of the flow comes from the horizon (Table 8). During discharge, the pressure drops to about 44 bar and the temperature to ~256°C. The initial temperature and pressure runs demonstrate that the reservoir contains sub-boiling fluid. The runs taken during discharge show that P and T are on the steam-water two-phase boundary and the decrease in pressure from static conditions proves that boiling starts in the formation during discharge.

In *well TR4C*, which is 2179 m deep, total loss of circulation during drilling occurred at 1752 m. Temperature at this depth was close to 275°C and pressure 100 bar (Figure 3 in Appendix I). The quartz and Na-K geothermometers indicated a feed zone with temperature of 278°C which is practically the same as the measured temperature at 1752 m, supporting the idea that most of the flow comes from the horizon (Table 8). Inspection of the temperature profiles at deep levels suggested that the well had not stabilized thermally when the profiles were taken (Figure 3, Appendix I) making deductions about initial conditions difficult. Partial circulation losses occurred below 1752 m depth. It is clear that the reservoir is sub-boiling, but during discharge the pressure drops considerably as well as the temperature (30 bar and ~240°C), demonstrating that extensive boiling starts in the aquifer. A reversal in temperature below 1900 m likely reflects that the well had not recovered thermally near the bottom when temperature measurements were carried out downhole; a partial loss occurred at 1761-2179 m.

In *well TR5*, which is 2086 m deep, total loss of circulation during drilling occurred at 1830-2086 m. Temperature at 1853 m depth was 305°C and the pressure 107 bar (Figure 4 in Appendix I). The quartz

and Na-K geothermometers indicated a feed zone temperature of 294°C which is reasonably close to the measured temperature at 1853 m, supporting the idea that most of the flow comes from this horizon (Table 8). During discharge, the pressure dropped to about 32 bar and the temperature to ~240°C. The initial temperature and pressure runs demonstrate that the reservoir contains sub-boiling water, yet very close to the boiling temperature at this depth. The runs taken during discharge showed that P and T were on the steam-water two-phase boundary and the decrease in pressure from static conditions proves that boiling starts in the formation during discharge. A clear reversal in temperature below 1900 m indicates a horizon of fluid loss close to the well bottom, which corresponds to the zone of partial losses which occurred at 1830-2086.

In *well TR5B*, which is 2097 m deep, total loss of circulation during drilling occurred at 2000 m. Temperature at this depth was 300°C and the pressure 140 bar, indicating sub-boiling conditions (Figure 5 in Appendix I). The quartz and Na-K geothermometers indicated a feed zone temperature of 281°C (Table 8), which is somewhat lower than the measured temperature at 2000 m, indicating that some inflow occurs at a shallower level. During discharge, the pressure dropped only slightly, or to about 110 bar and the temperature to ~275°C. This demonstrates that boiling starts in the well when producing.

Total loss of circulation during the drilling of *well TR5C* occurred at 1996-2343 m depth. A maximum temperature of 294°C was recorded at 1817-1909 m depth with a pressure of 100 bar (Figure 6 in Appendix I). The quartz and Na-K geothermometers indicated a feed zone temperature of 277°C, which is somewhat below the measured temperature at 1817 m, indicating some production from aquifers at shallower depth (Table 8). The temperature and pressure runs taken on 23 May and 08 June 2012 were carried out just after acid stimulation and mechanical cleaning of the well when it had started to heat up. These runs, therefore, did not provide information on the thermally stabilized well nor on conditions during discharge. Inspection of other temperature profiles suggested the existence of two producing aquifers at 1900 and 2100 m (Figure 6, Appendix I). During discharge, the pressure and temperature decreased to around 30 bar and 230°C, respectively, showing that boiling starts in the formation during discharge.

In *well TR9*, which is 2298 m deep, total loss of circulation during drilling occurred at 1663 m. Temperature at this depth was 281°C and the pressure 120 bar (Figure 7 in Appendix I). Therefore, the deep reservoir fluid is sub-boiling. The quartz and Na-K geothermometers indicated a feed zone temperature of 274°C; which is reasonably close to the measured temperature at 1663 m, supporting the idea that most of the flow comes from that horizon (Table 8). Logging tools became trapped at 1300 m depth which caused a restriction causing a pressure drop pressure and decrease in flow. This restriction has now been removed but the available logging data are from a period before the removal. Inspection of the temperature profiles at deep levels suggested the existence of several producing aquifers at depths of 1400, 1500 and 1900 m (Figure 7, Appendix I). During discharge, the pressure and temperature did not change, staying around 100 bar and ~280°C, respectively, so the first depth level of boiling is within the well.

Well TR17 is 2600 m deep. Data for lost circulation during drilling were not available. The maximum temperature was 258°C (Figure 8 in Appendix I). The quartz and Na-K geothermometers indicated a feed zone temperature of 262°C, which is the same as the measured one, well within the limits of error (Table 8). During discharge, the pressure rotated defining a pivot point at 1350 m. Below this depth, the temperature stayed constant to the bottom of the well at ~258°C suggesting a down flow from the aquifer at 1350 m. Temperature and pressure runs demonstrated that the reservoir contains sub-boiling fluid. Yet, at aquifer depth, it was very close to the boiling point.

In *well TR17A*, which is 2690 m deep, total loss of circulation during drilling occurred at 2000 m. No temperature and pressure loggings were available during heating-up of this well which was completed in early 2004. After heating-up, the temperature at 2000 m depth was 286°C and the pressure was 96 bar (Figure 9 in Appendix I), indicating that the reservoir was sub-boiling. A strong reversal was observed below 2000 m that has persisted for 5 years, likely reflecting a reversal in reservoir

temperature. The quartz and Na-K geothermometers indicated a feed zone temperature of 244°C which is reasonably close to the measured temperature at 2000 m, supporting the idea that most of the flow comes from this horizon (Table 8). During discharge, the pressure dropped to about 88 bar and the temperature to ~240°C, so boiling starts in the well during discharge.

Well TR18 was drilled to a depth of 2660 m. Total loss of circulation occurred at 1875-2660 m. The maximum measured temperature in this depth was 263°C and the pressure ~140 bar, indicating sub-boiling conditions (Figure 10, Appendix I). Pressure and temperature did not change at this depth during discharge, showing that the first depth level of boiling is within this well at around 1000 m. Quartz and Na-K geothermometer temperatures were 257 and 246°C, respectively (Table 8), very similar to the measured temperature at the depth level of the feed zones.

Well TR18AST is shallow, 1085 m deep with a maximum temperature of 248°C. It discharges vapour only at a wellhead pressure of 38 bars, indicating a possible vapour zone that could have developed on top of the liquid reservoir as a consequence of pressure drawdown by exploitation. This steam has close to maximum enthalpy.

4.2 Discharge enthalpy

The discharge enthalpy of the wells was measured using the Russell James method which involves recording critical lip pressure (P^c) and water flow from an atmospheric silencer. The measured values are shown in Table 8. They are similar to, or slightly higher than that of steam-saturated water at measured downhole temperatures and the estimated aquifer temperatures by chemical geothermometers. The critical lip pressure method tends to give high results. The reason is that some water may be removed from the silencer with steam, leading to low values for water flow from the silencer. In some of these wells where measured enthalpy is slightly above that of steam-saturated water at the estimated aquifer temperature, the first depth of boiling during discharge is within the well, proving that only liquid water enters these wells. On the basis of this observation, it was concluded that all wells at Berlín, except for the dry steam well TR18A, truly have liquid enthalpy. With possible further pressure drawdown in the reservoir in the future, the first depth level of boiling may move from the wells into the formation. Such a change could be accompanied by an increase in well discharge enthalpy, at least if extensive boiling starts in the aquifer relatively far from the well.

5. AQUIFER FLUID COMPOSITION

5.1 Modelling

Based on the conclusions in Chapter 4 that well discharge enthalpy is that of steam saturated water in feed zones, it follows that both total well discharge compositions and discharge enthalpy are the same as those of the aquifer fluid, i.e.

$$M^{d,t} = M^{d,l} + M^{d,v} = M^{f,l} \tag{1}$$

and

$$h^{d,t} \cdot M^{d,t} = h^{d,l} \cdot M^{d,l} + h^{d,v} \cdot M^{d,v} = h^{f,l} \cdot M^{f,l} \tag{2}$$

In Equations 1 and 2, M designates fluid flow (kg/s), h is specific enthalpy (kJ/kg) and the superscripts d, l, v and t indicate discharge, liquid water, vapour and total discharge, respectively.

By dividing Equation 2 by $M^{d,t}$ we obtain:

$$h^{d,t} = h^{d,l} \cdot \left(1 - x^{d,v}\right) + h^{d,v} \cdot x^{d,v} = h^{f,l} \tag{3}$$

Here, $x^{d,v}$ denotes the vapour fraction in the discharge at the wellhead (at the pressure at which the samples were collected).

Rearrangement and isolation of $x^{d,v}$ leads to

$$x^{d,v} = \frac{h^{f,l} - h^{d,l}}{h^{d,v} - h^{d,l}} \tag{4}$$

From the evaluation of the aquifer temperature and measurement of sampling pressure (vapour pressure), all the enthalpy values in Equation 4 can be obtained from steam tables, allowing $x^{d,v}$ to be calculated.

For the concentration of any chemical component (m_i) we have

$$m_i^{d,t} = m_i^{f,l} = m_i^{d,l}\left(1 - x^{d,v}\right) + m_i^{d,v} x^{d,v} \tag{5}$$

By analysing the concentrations of component i in both liquid and vapour phases collected at the wellhead, its concentrations in the aquifer fluid can be obtained from Equation 5. Some components in the aquifer fluid (dissolved solids) occur in negligible concentrations in the vapour phase. Therefore, they are not even analysed for. Gases with low solubility in water, such as H_2, CH_4 N_2, O_2 and many others, practically partition completely into the vapour phase. In the former case $m_i^{d,v}=0$, and $m_i^{d,l}=0$ in the latter.

The WATCH chemical speciation program (Arnórsson et al., 1982), version 2.4 (Bjarnason, 1994,) was used to calculate aquifer water compositions and aqueous species distribution. The latter allows activity products to be retrieved for minerals and, together with knowledge of mineral solubility constants from chemical thermodynamic data, saturation for selected hydrothermal minerals in producing aquifers was calculated. Aquifer temperatures were selected on the basis of the measured downhole temperatures in thermally stabilized wells, combined with circulation losses during drilling, and the quartz and Na-K chemical geothermometer results. This is discussed in Section 5.2 below.

5.2 Selection of aquifer temperature

The use of dissolved silica as a geothermometer is based on experimentally determined solubility of quartz in pure water (Fournier and Potter, 1982a and b; and Gunnarsson and Arnórsson, 2000). The dissolution reaction for quartz (and other silica mineral species) is generally expressed as:

$$SiO_{2,quartz} + 2H_2O = H_4SiO^0_{4,aq} \tag{6}$$

It has been well established that the solubility of quartz controls dissolved silica in geothermal reservoir waters when temperatures exceed 120-180°C. The earliest silica (quartz) geothermometer calibration, proposed by Fournier and Rowe (1966), covered the range 120-330°C. Later, Fournier and Potter (1982a and b) presented an equation for the quartz solubility constant over a larger temperature, as well as a pressure range. This equation is the most widely used. Gunnarsson and Arnórsson (2000) carried out measurements of amorphous silica solubility over a wide range of temperatures, calculated the standard Gibbs energy of the $H_4SiO_{4,aq}^0$ and revised the quartz solubility, taking into account all experimental data and making it consistent with amorphous silica solubility. The quartz solubility curve of Gunnarsson and Arnórsson (2000) was used in this report. From 50 to 250°C, it is practically the same as that of Fournier and Rowe (1966) and Fournier and Potter (1982a and b), but at higher temperatures it is lower, the difference being quite significant above 300°C. Figure 4 summarizes all experimental data on quartz solubility. As can be seen from this figure, there is an inconsistency in the experimental results at high temperatures. This inconsistency calls for additional experiments on the solubility of quartz in pure water to resolve the observed inconsistency.

The calibration of the Na-K geothermometer is based on published chemical thermodynamic data on the stable alkali feldspars (low-albite and microcline) at low temperature, summarized by Arnórsson (1999). The calibration curve is given by Arnórsson et al. (2000). This curve is quite similar to many earlier geochemical calibrations (Arnórsson et al., 2000). With improved internally consistent data bases on minerals and aqueous species, it is considered that calibration based on reliable chemical thermodynamic data is preferred to empirical (geochemical) calibration. The latter was, however, justified when available thermodynamic data were found to be inadequate.

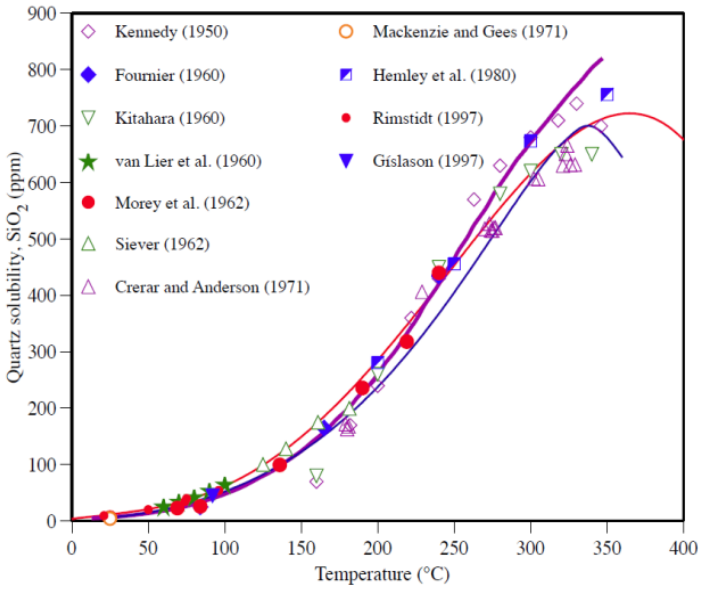

FIGURE 4: Quartz solubility
(Gunnarsson and Arnórsson, 2000)

As can be seen from Table 8, circulation losses were reported at various depths in the Berlín geothermal field. All these losses may not represent a permeable zone. An earlier zone at a shallower depth may have re-opened, especially since fluid circulation halted when additional drill strings were being added. Continued circulation loss indicates that the loss zone did not seal upon continued drilling. It gives no information about the well conditions below this zone.

Temperature runs after well completion and when the well was heating up provide important information about potential aquifers. They may show up as negative or positive temperature peaks. Chemical geothermometers, on the other hand, provide some kind of an average aquifer temperature of the fluid flowing into wells. By combining all of these data, the best concept is attained on the depth level of feed zones producing into discharging wells.

The boiling point curve with depth is steep at temperatures above ~260-270°C because above these temperatures the boiling point of water increases slowly with increasing pressure (depth). At Berlín, the feed zone temperatures of the wells are most often over 260°C. For this reason, one can expect measured temperatures at the depth levels of feed zones to compare well with geothermometers, as is the case.

6. SPECIATION DISTRIBUTION

The WATCH chemical speciation program (Arnórsson et al., 1982) version 2.4 (Bjarnason, 1994) was used to calculate the aquifer fluid composition and individual speciation distributions. It was assumed that all the wells for which analytical data are shown in Table 7 had liquid enthalpy, in which case the aquifer fluid composition is the same as that of the total well discharge. The temperature of the aquifer fluid was based on results of measured downhole temperatures and the quartz and Na-K geothermometer temperatures. The results for the calculated aquifer fluid compositions and the concentrations of individual aqueous species are in Appendix II which is published in a separate report (Hernández, 2012).

The aquifer water pH at the selected aquifer temperature lies in the range 5.0-5.9. Samples with the lowest and highest measured pH, respectively, yielded the lowest and highest aquifer water pH. As discussed in the following chapter, the Saturation Index for minerals with pH-dependent solubility varies with the calculated aquifer water pH, increasing with increasing pH. This correlation suggests that the

measured pH of samples, for samples with high pH, is in error, most likely due to sample degassing with respect to CO_2 and H_2S prior to measurement of the pH. Calculations by the WATCH program showed that the samples were unstable, with higher CO_2 partial pressures than the atmosphere. Thus, the samples tended to degas upon storage. Samples containing H_2S are always unstable with respect to this gas, because H_2S concentrations in the air are practically zero. The above described results indicate that samples for pH-measurement must be cooled and collected separately into air-tight glass bottles for pH measurements that must be carried out as soon as possible after collection, preferably on site. Cooling is necessary because if a hot sample is collected into an air-tight glass bottle it will contract upon cooling, thus favouring degassing.

The pH has been discussed is some detail because of the interest in studying sulphide mineral scaling in wells in the Berlín field. Sulphide minerals have pH-dependent solubility. For that reason, accurate evaluation of their saturation state in the aquifer water requires accurate calculation of the aquifer water pH, hence accurate measurement of pH of water samples. Subsequent to calculation of the aquifer water speciation distribution, it is possible to assess with the aid of the WATCH program how the saturation state of the fluid, with respect to minerals, changes when the water boils and degasses.

Studies indicate that fluids in high-temperature geothermal systems are generally close to being calcite saturated. At Berlín, there is considerable scatter in the calculated SI-indices for calcite, varying between +0.48 and -0.96, the average being -0.34 corresponding to just over twofold under-saturation. It is quite possible that the large scatter is, at least to some extent, a reflection of error in the pH measurements of the water samples, because the calcite Saturation Index varies in a rather regular manner with the calculated aquifer water pH, emphasizing again the importance of accurate measurement of the H^+ species.

Inherent to the WATCH program, like other such programs, is that a specific temperature needs to be selected for the speciation calculations. Of course, wells may have multiple feeds of different temperatures, in which case there is no fluid in the reservoir that exactly matches compositionally the total well discharge at the selected aquifer temperature, i.e. the temperature selected for the WATCH program to calculate individual aqueous species activities. At Berlín, producing aquifers of individual production wells have similar temperatures, as indicated by both measured downhole temperatures in wells and geothermometer results. For that reason, the calculated results obtained by the WATCH program were considered quite reliable, depending on the quality of the thermodynamic data base of the program.

The thermodynamic database for the speciation calculations by WATCH is that presented by Arnórsson et al. (1982), except for gas solubility, Al-hydroxide and ferrous and ferric hydroxide dissociation constants, which were taken from Fernandez-Prini et al. (2003), Arnórsson and Andrésdóttir (1999) and Arnórsson et al. (2002), respectively. Further, the dissociation constant for $CaHCO_3^+$ is based on the experimental data (0–90°C) of Plummer and Busenberg (1982) and extrapolated to higher temperatures using the electrostatic approach of Helgeson (1967).

7. MINERAL SATURATION

7.1 Background

Essentially, three ways are used to express mineral-solution equilibria in natural water-rock systems. One involves the use of mineral phase diagrams which shows the stability fields of minerals as a function of specific aqueous species activities or activity ratios. Another is to show saturation as a Saturation Index and to plot it against a variable such as pH or temperature. The Saturation Index (SI) for a given chemical reaction is defined as:

$$SI = \frac{\log Q}{\log K} \tag{7}$$

where K is the equilibrium constant for a given reaction and Q is the activity product.

Q is given by:

$$Q = \frac{a_A^a \cdot a_B^b}{a_C^c \cdot a_D^d} \tag{8}$$

for reaction

$$cC + dD = aA + bB \tag{9}$$

where the reactants are species C and D and the products species A and B. The lower case letters designate the stoichiometric coefficients of the respective chemical species.

The third way to express mineral saturation is to plot Q (usually as log Q) against a variable, such as temperature or pH, and draw up a curve on the diagram that represents the equilibrium constant. The thermodynamic definition of equilibrium is described by the following equation:

$$\Delta G_r = \Delta G_r^o + RT\ln Q \tag{10}$$

where ΔG_r^o stands for the standard Gibbs energy of reaction, equal to –RTlnK.

At equilibrium, the Gibbs energy of reaction is zero ($\Delta G_r = 0$), so K = Q at equilibrium. This implies that SI = 0 at equilibrium, but is positive for over-saturated solutions and negative for under-saturated solutions. When using log Q in the plot, the Q plots on the equilibrium curve at equilibrium, above the curve in the case of super-saturation and below the curve for under-saturation. In this contribution, it was chosen to plot Q against temperature or pH and to draw up the equilibrium curve.

The mineral saturation state was evaluated for 10 common hydrothermal minerals in high-temperatures in the Berlín geothermal system. These minerals are listed in Table 9, together with an expression used

TABLE 9: Temperature equations for equilibrium constants for individual mineral dissolution reactions, valid in the range 0-350 °C at Psat; unit activity was selected for all minerals and liquid water

	Reaction	LogK(T)
1	and+4H^++8H_2O=3Ca^{+2}+2$Fe(OH)_4^-$+3$H_4SiO_4^0$	+940.225−15419.3/T+0.58092T−0.0002971T^2−421.727 logT
2	cal+2H+=Ca^{+2}+H_2O_l+$CO_{2,aq}$	−68.271+4385.24/T−0.007525T+25.856 logT
3	czo+12H_2O_l=2Ca^{+2}+3 $Al(OH)_4^-$+3$H_4SiO_4^0$ +OH^-	+36.052−6854.78/T+0.13236T−0.00013749T^2−33.508 logT
4	epi+12H_2O_l=2Ca^{+2}+$Fe(OH)_4^-$+2$Al(OH)_4^-$+3$H_4SiO_4^0$+OH^-	+893.547−27077.4/T+0.54124T−0.0003022T^2−398.380 logT
5	flu=Ca^{+2}+2F^-	+66.54−4318/T−25.47 logT
6	gro+4H^++8H_2O_l=3Ca^{+2}+2$Al(OH)_4^-$+3$H_4SiO_4^0$	−517.662+17623.7/T−0.14343T+203.808 logT
7	mag+4H_2O_l=2$Fe(OH)_4^-$+Fe^{+2}	+949.951−24258.2/T+0.51474T−0.0002402T^2−417.136 logT
8	pre+10H_2O_l=2Ca^{+2}+2$Al(OH)_4^-$+3H_4 SiO_4^0+2OH^-	+833.950−25642.8/T+0.5035T−0.0002941T^2−369.297 logT
9	pyr+2H^++$H_{2,aq}$=2H_2S_{aq}+Fe^{+2}	−1.397−461.30/T−0.0009128T+1.626 logT
10	pyrr+2H^+=H_2S_{aq}+Fe^{+2}	−3.043+1579.06/T+0.001987T+0.120 logT
11	qtz+2H_2O_l=$H_4SiO_4^0$	−34.188+197.47/T−5.851·10−6T^2+12.245 logT
12	wol+2H^++H_2O_l=Ca^{+2}+H 4SiO_4^0	−127.096+8151.38/T−0.02981T+49.282 logT

The thermodynamic properties of $CO_{2,aq}$, H_2S_{aq} and $H_{2,aq}$ were retrieved from Fernandez-Prini et al. (2003).
Data on minerals are from Holland and Powell (1998), except pyrite and pyrrhotite from Robie and Hemingway (1995).
The thermodynamic data on $H_4SiO_4^0$ and quartz solubility are from Gunnarsson and Arnórsson (2000), those on H_2O_l, Ca^{+2}, Fe^{+2} and OH^- from SUPCRT92 program (Johnson et al., 1992) using the slop98.dat data set.
The data on $Fe(OH)_4^-$ and $Al(OH)_4^-$ are from Diakonov et al. (1999) and Pokrovskii and Helgeson (1995), respectively.
The fluorite solubility equation is from Arnórsson et al. (1982) and is based on Nordstrom and Jenne (1977).
The mineral phases have the following meanings: and: andradite; cal: calcite; czo: clinozoisite; epi: epidote; flu: fluorite; gro: grossular; mag: magnetite; pre: prehnite; pyr: pyrite; pyrr: pyrrhotite; qtz: quartz; wol: wollastonite.

for each reaction. The temperature dependence for the equilibrium constants is also shown in the table. They are taken from Karingithi et al. (2010) and are valid at 1 bar below 100°C and at vapour saturation pressures at higher temperatures. In Table 10, mineral pairs and mineral assemblage reactions and the temperature dependence for the equilibrium constants are listed. The Q values for all these reactions were calculated with the aid of the WATCH speciation program, assuming liquid enthalpy for the reservoir fluid with a temperature shown as "selected temperature" in Table 8, based on information about circulation losses during drilling, temperature logging in thermally stabilized wells and the quartz and Na-K geothermometers.

TABLE 10: Temperature equations for the equilibrium constants for mineral pairs and mineral assemblage reactions that may control calcium/proton a_{Ca+2} / a_{H+}^2, ferric-hydroxide/hydroxide $a_{Fe(OH)4-} / a_{OH-}$ ($aFe(OH)_4^-$ / aOH^-), hydrogen sulphide/hydrogen (aH_2S_{aq} / $aH_{2,aq}$) activity ratios and gas concentrations in solution; equations are valid in the range 0–350 °C at Psat; unit activity was selected for all minerals and liquid water.

Species activity		Reaction	LogK (T)
1	$a_{Ca^{+2}}/{a_{H^{+2}}}^2$	$\frac{3}{5}$gro + $2H^+ = \frac{4}{5}H_2O + \frac{2}{5}$czo + $\frac{3}{5}$qtz + Ca^{+2}	2.971+263838/T²+2642.9/T−0.003066T−0.000003885T²+0.797 logT
2	$a_{Ca^{+2}}/{a_{H^{+2}}}^2$	$\frac{3}{2}$pre + $2H^+$ = czo + 32qtz + $2H_2O + Ca^{+2}$	2.643+335608/T²+1550.1/T+0.0006563T−0.000006123T²+0.870·logT
3	$a_{Ca^{+2}}/{a_{H^{+2}}}^2$	wol + $2H^+$ = qtz + H_2O_l + Ca^{+2}	3.047+302461/T²+3088.8/T−0.004542T−0.000002571T² +0.748·logT
4	$a_{Fe(OH)_4^-}/a_{OH^-}$	epi + OH^- + $2H_2O_l$ = pre + $Fe(OH)_4^-$	2.786+132357/T²+1144.9/T+0.0002260T+0.000008115T²−0.933·logT
5	$a_{Fe(OH)_4^-}/a_{OH^-}$	epi + wol + OH− + H2Ol = qtz + gro + FedOHÞ−4	−2.935+177922/T²−1210.84/T+0.0004109T+0.000008970T²−0.978·logT
6	$a_{Fe(OH)_4^-}/a_{OH^-}$	$\frac{1}{2}$mag + $\frac{5}{3}H_2O + OH^- = Fe(OH)_4^- + \frac{3}{2}H_{2;aq}$	−1.452+21398.6/T²−671.80/T−0.00008861T+0.000005453T²−0.486·logT
7	$a_{Fe(OH)_4^-}/a_{OH^-}$	$\frac{1}{2}$hem + $\frac{3}{2}H_2O_l + OH^- = Fe(OH)_4^-$	−2.675+127537/T²−1494.6/T+0.0020402T+0.000007393T²−0.817·logT
8	$a_{H_2S_{aq}}/a_{H_{2,aq}}^{1/3}$	$\frac{1}{2}$pyr + $\frac{1}{3}H_{2;aq} + \frac{2}{3}H_2O_l = \frac{1}{6}$mag + H_2S_{aq}	12.225+500528/T²−7771.49/T−0.038468T +0.00002424T²+4.546 logT
9	$a_{H_2S_{aq}}/a_{H_{2,aq}}$	pyr − $H_{2,\,aq}$ = pyrr + H_2S_{aq}	0.549−124186/T²−972.20/T+0.0036744T−0.000003227T²+0.383·logT
10	CO_2	czo + cal + $\frac{3}{2}$qtz + $H_2O_l = \frac{3}{2}$pre + $CO_{2;aq}$	−0.890+7251.5/T²−1710.6/T+0.004188T+0.000002683T²−0.064 logT
11	CO_2	$\frac{2}{5}$czo+ cal+ $\frac{3}{5}$qtz = $\frac{3}{5}$gro + $\frac{1}{5}H_2O_l + CO_{2;aq}$	−1.449−40536/T²−2135.9/T+0.0065639T+0.000002725T²−0.193 logT
12	H_2S	$\frac{1}{3}$pyr + $\frac{1}{3}$pyrr + $\frac{2}{3}$pre + $\frac{2}{3}H_2O_l = \frac{2}{3}$epi + H_2S_{aq}	13.608+592324/T²−9346.7/T−0.043552T+0.000029164T²+5.139 logT
13	H_2S	$\frac{2}{3}$gro + $\frac{1}{3}$pyr + $\frac{1}{3}$pyrr+ $\frac{2}{3}$qtz + $\frac{4}{3}H_2O_l = \frac{2}{3}$epi + $\frac{2}{3}$wol + H_2S_{aq}	13.659+555082/T²−9256.6/T−0.043608T+0.000028613T²+5.148 logT
14	H_2S	2gro + $\frac{1}{4}$pyr + $\frac{1}{2}$mag + 2qtz + $2H_2O_l$ = 2epi + 2wol + H_2S_{aq}	−0.836−216659/T²−2847.3/T+0.008524T−0.000002366T²+0.152 logT
15	H_2S	$\frac{1}{4}$pyr + $\frac{1}{2}$pyrr + $H_2O_l = \frac{1}{4}$mag + H_2S_{aq}	13.589+590215/T²−9024.5/T−0.044882T+0.000029780T²+5.068 logT
16	H_2	$\frac{4}{3}$pyrr + $\frac{2}{3}$pre+ $\frac{2}{3}H_2O_l = \frac{2}{3}$epi + $\frac{2}{3}$pyr + $H_{2;aq}$	−1.640−124524/T²−777.19/T−0.0005501T+0.000007756T²−0.565 logT
17	H_2	$\frac{2}{3}$gro+ $\frac{4}{3}$pyrr+ $\frac{2}{3}$qtz + $\frac{4}{3}H_2O_l = \frac{2}{3}$epi + $\frac{2}{3}$wol + $\frac{2}{3}$pyr + $H_{2;aq}$	−1.544−151109/T²−752.389/T−0.0005868T+0.000007080T²−0.532 logT
18	H_2	6gro + 2mag + 6qtz + $4H_2O_l$ = 6epi + 6wol + $H_{2,\,aq}$	1.444−273812/T²−3962.1/T+0.002401T+0.000001304T²+0.979 logT
19	H_2	$\frac{2}{3}$pyr + $H_2O_l = \frac{3}{4}$pyr + $\frac{1}{4}$mag + $H_{2;aq}$	−1.654−95456.8/T²−621.84/T−0.001257T+0.000007569T²−0.600 logT

The sources of the thermodynamic data used to obtain the temperature equations are given in the footnote of Table 9.

7.2 Results

7.2.1 Calcite

Reactions involving calcite and aqueous solutions are relatively rapid. Therefore equilibrium is expected to be closely approached between calcite and solution in geothermal systems, especially when they have high temperatures (Arnórsson, 1978,1991; Arnórsson et al., 2002; Karingithi et al., 2010). Yet, under-saturation may prevail in some systems due to an inadequate supply of CO_2 to the fluid to saturate it with calcite.

The results for calcite are shown in Figure 5a. They indicate over-saturation for most of the wells. The degree of over-saturation increases with increasing aquifer water pH (Figure 5b). At the lowest pH-values, 5.1-5.2 over-saturation is insignificant. As already discussed, the relationship of the degree of over-saturation with pH is considered to reflect faulty measurements of the pH of water samples.

However, this needs to be verified by carefully measuring pH on site when the samples are collected, and as soon as possible after the samples have arrived at the chemical laboratory and, subsequently, to demonstrate how much it might change upon storage. If it is assumed that the measured pH values are generally high; the conclusion follows that the aquifer water at Berlín is close to calcite saturation.

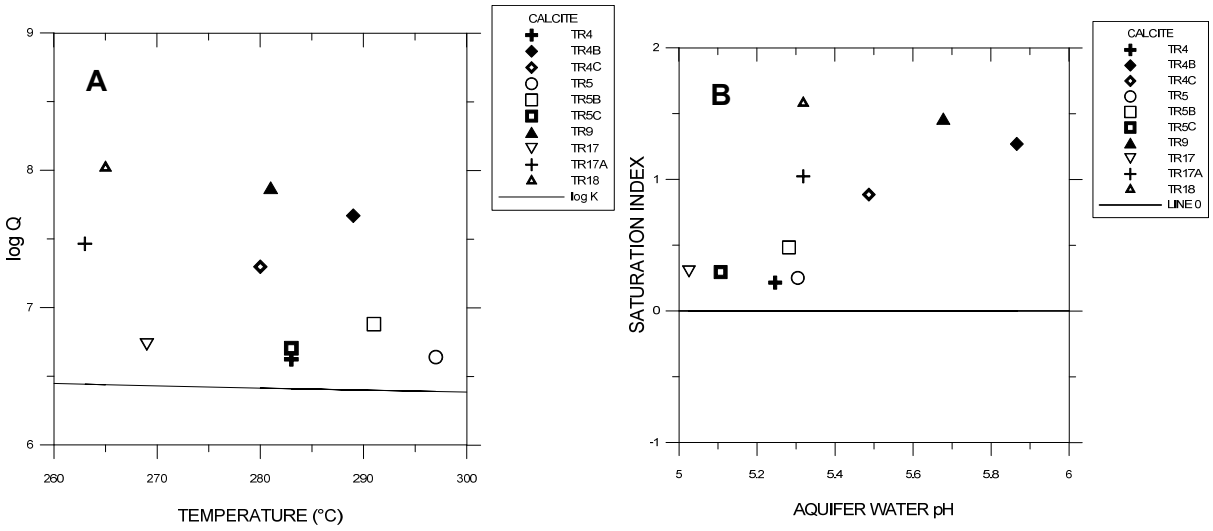

FIGURE 5: a) LogQ and LogK calcite against temperature; b) SI calcite against aquifer water pH

7.3 pH dependence of silicate mineral solubility

Like calcite, all the silicate minerals considered for the present study have pH dependent solubility; their solubility decreases with increasing pH. This is demonstrated by the following reaction for prehnite:

$$Ca_2Al_2Si_3O_{10}(OH)_2 + 10H^+ = 2Ca^{+2} + 2Al^{+3} + 3H_4SiO_4 \qquad (11)$$

What is common with all pH dependent mineral-dissolution reactions is that such reactions involve the consumption of protons; these mineral precipitation reactions could, on the other hand, consume OH^- to lower water pH. Figures 6 to 11show the saturation state for all the silicate minerals considered for the present study: prehnite and wollastonite, the end members of epidote solid solutions, epidote and as well as andradite and grossular of garnet solid solution. The aquifer water at Berlín shows considerable scatter from under- to over-saturation for grossular-garnet, but systematic over-saturation for other

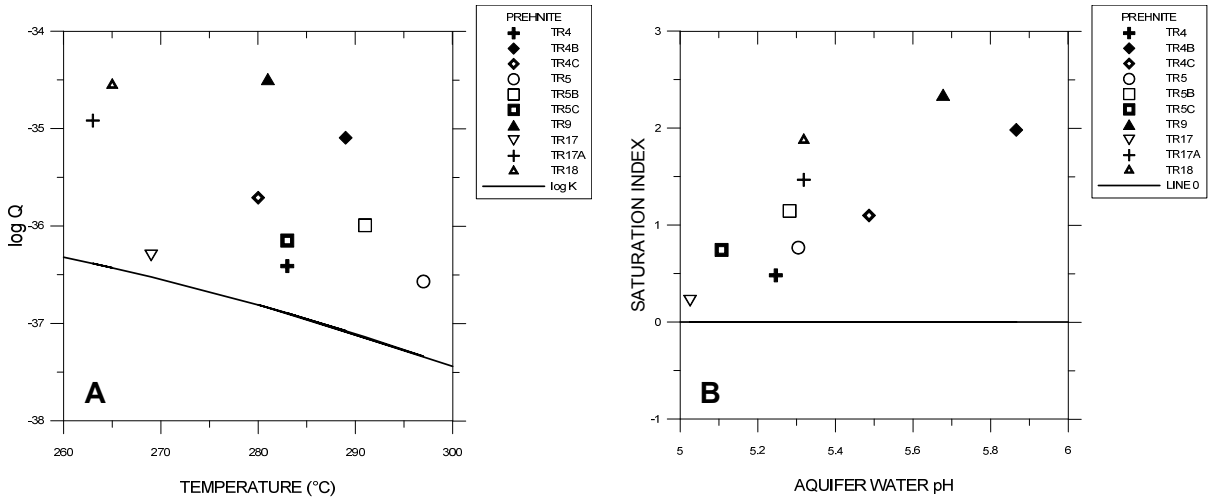

FIGURE 6: a) LogQ and LogK prehnite vs. temperature; b) SI prehnite vs. aquifer water pH

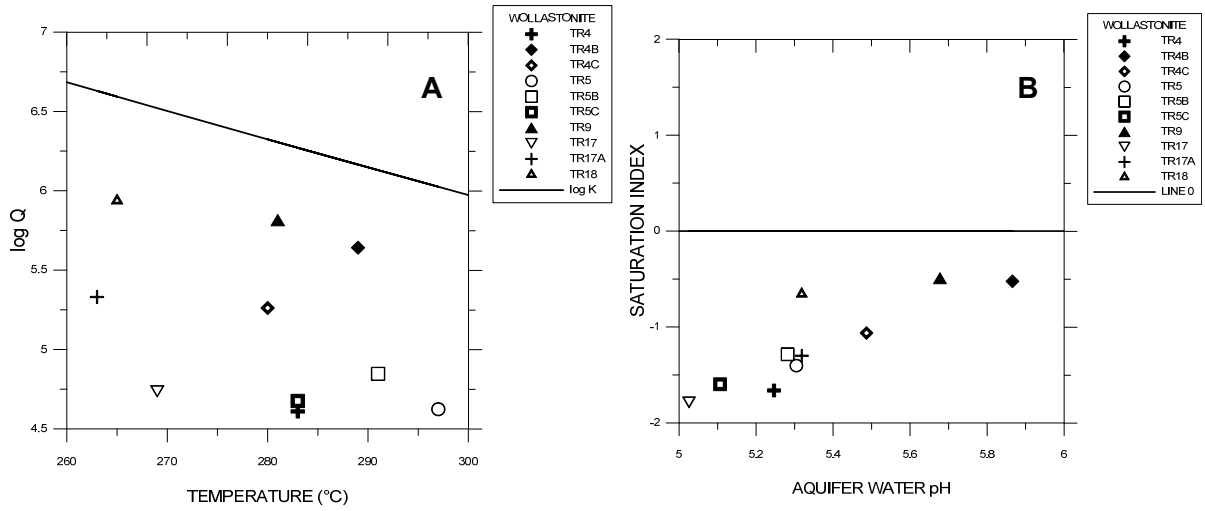

FIGURE 7: a) LogQ and LogK wollastonite vs. temperature;
b) SI wollastonite vs. aquifer water pH

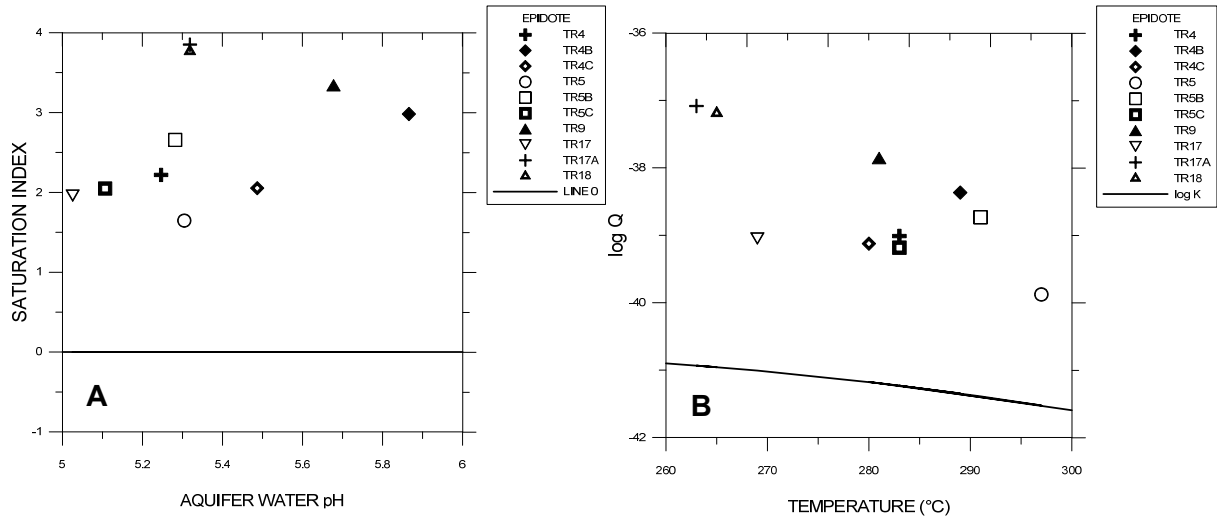

FIGURE 8: a) LogQ and LogK epidote vs. temperature; b) SI epidote vs. aquifer water pH

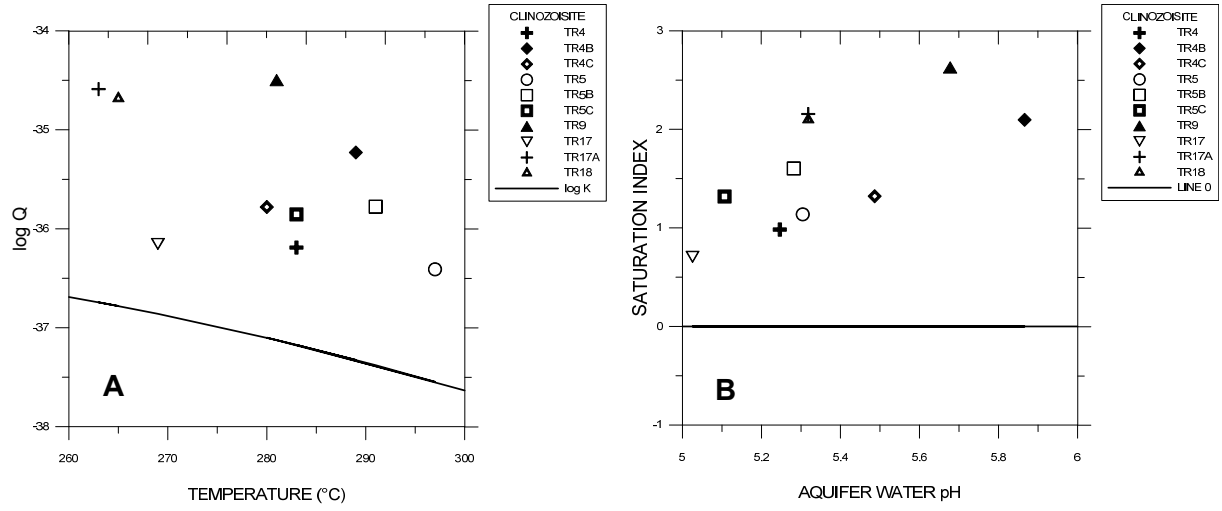

FIGURE 9: a) LogQ and LogK clinozoisite vs. temperature; b) SI clinozoisite vs. aquifer water pH

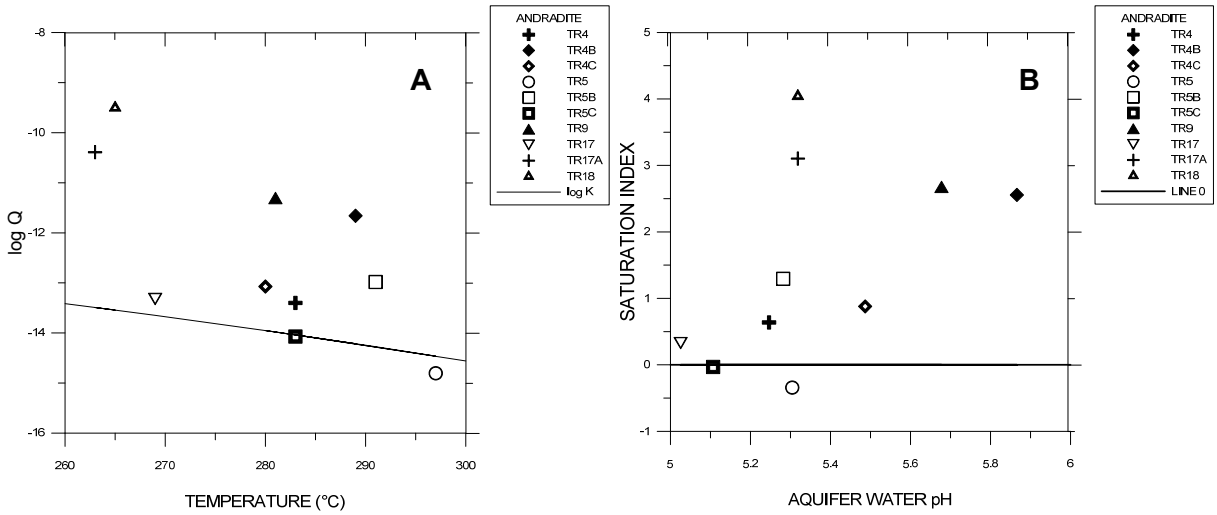

FIGURE 10: a) LogQ and LogK andradite vs. temperature; b) SI andradite vs. aquifer water pH

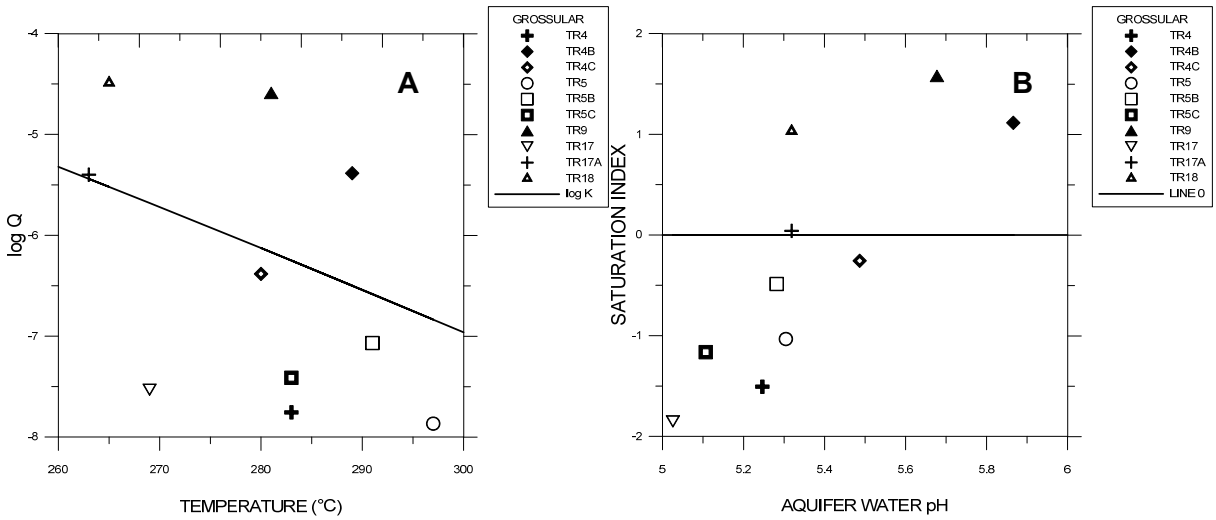

FIGURE 11: a) LogQ and LogK grossular vs. temperature; b) SI grossular vs. aquifer water pH

calcium bearing silicate minerals, except for wollastonite which is systematically under-saturated. This suggests that wollastonite is not stable. To express it differently, the water is under-saturated with respect to this mineral. Therefore, it does not form. Andradite is usually under-saturated.

For solid solution silicate minerals, an accurate assessment of their saturation states requires knowledge of their composition. Unfortunately, such data are not available for the Berlín geothermal field. The variable degree of over-saturation for the iron bearing silicates is, as pointed out by Karingithi et al. (2010), an artefact produced by inadequate data on the thermodynamic properties of aqueous iron-hydroxy species that leads to overestimation of the concentration of the $Fe(OH)^{-}_{4}$ species.

7.4 Iron bearing sulphide and oxide minerals

The saturation state of the aquifer water at Berlín was evaluated with respect to pyrite (FeS_2), pyrrhotite (FeS) and magnetite (Fe_3O_4). For pyrrhotite the calculated activity product ranged from significant under-saturation to strong over-saturation (Figure 12). Half of the waters were close to saturation. The log Q values increased regularly with decreasing aquifer temperature. This variation may be the

consequence of erroneous thermodynamic data on the Fe-hydroxide aqueous species, Fe^{+2} being underestimated at the highest temperatures but over-estimated at the lowest temperatures (<270°C). No correlation was observed between the saturation state and calculated aquifer water pH. The calculated degree of pyrrhotite over-saturation, in particular in three of the samples, could be correlated with the iron concentration in the samples. Iron contamination is always likely to occur, from sampling equipment, piping material or small rock fragments that pass through the filter membrane, the reason largely being the low iron concentration in hydrothermal fluids. It was, thus, concluded that the Berlín aquifer waters were close to being pyrrhotite saturated.

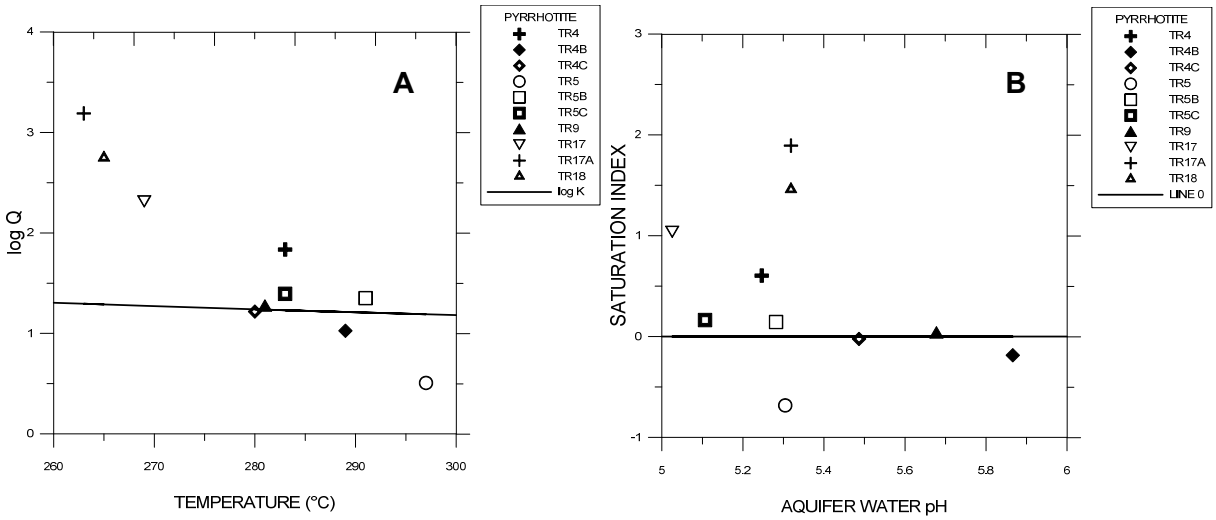

FIGURE 12: a) Log Q and Log K pyrrhotite vs. temperature; b) SI pyrrhotite vs. aquifer water pH

When considering the aquifer waters that are close to pyrrhotite saturation and, at the same time, relying on samples not contaminated with iron, it is evident that the aquifer water at Berlín was calculated to be pyrite under-saturated by ~ 2 orders of magnitude, suggesting that pyrite is not stable in the reservoir (Figure 13). The reaction for pyrite dissolution/precipitation is an oxidation-reduction reaction. Such an equilibrium may not have been closely approached, as is known to be the case for H_2S and SO_4 in many geothermal systems. A rigorous test of the pyrite saturation state requires the analysis of sulphur species with a valency of -1 like S_2^{-2}.

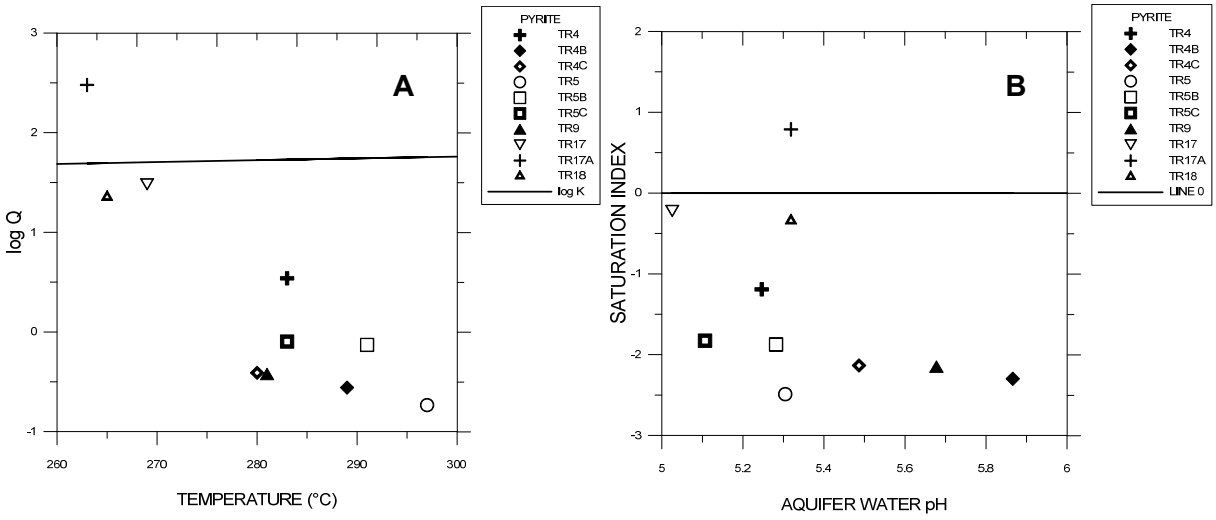

FIGURE 13: a) Log Q and Log K pyrite vs. temperature; b) SI pyrite vs. aquifer water pH

The Berlín aquifer water displays a large range of activity product (Q) values from over- to under-saturation with respect to magnetite (Figure 14). The over-saturated data points were those which were

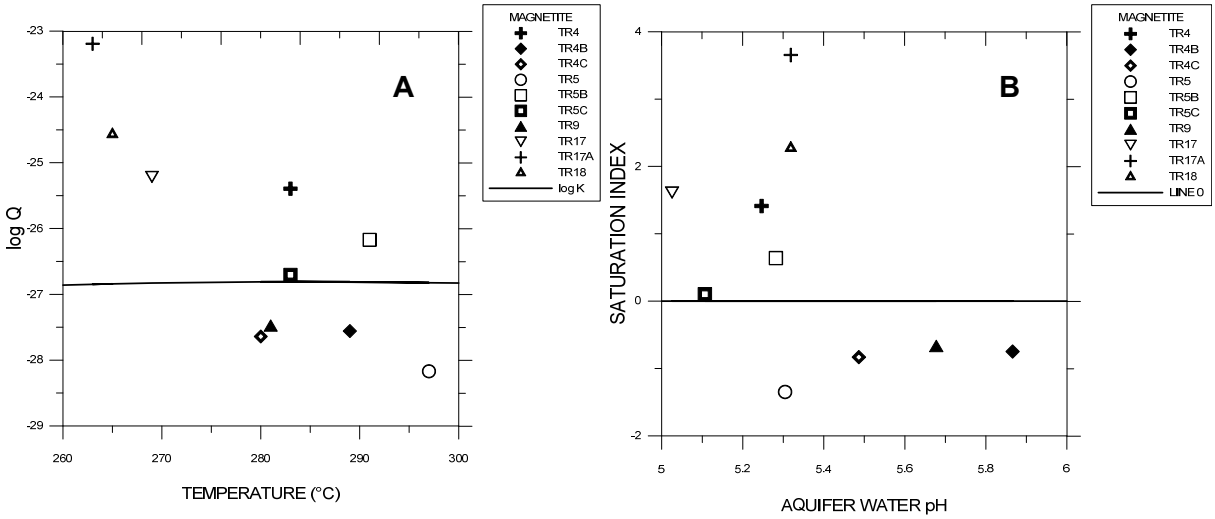

FIGURE 14: a) Log Q and Log K magnetite vs. temperature; b) SI magnetite vs. aquifer water pH

based on iron-contaminated samples. Other samples plotted relatively close to magnetite saturation. From this it is concluded that the reservoir water at Berlín likely is close to equilibrium with magnetite. As pointed out by Arnórsson et al. (2002) and Karingithi et al. (2010), the available experimental data on iron hydrolysis constants were inadequate, particularly in the case of high pH leading to an overestimation of $Fe(OH)_4^-$ and a corresponding underestimation of Fe^{+2}. In an effort to eliminate the suspected error in the thermodynamic properties of iron-hydroxide aqueous species, a pair of these two minerals was considered simultaneously to evaluate whether could be in simultaneous equilibrium with the aquifer water in which case the individual minerals must also be so.. Common equilibrium for pyrite and pyrrhotite is described by the following reaction:

$$FeS_2 + H_{2,aq} = FeS + H_2S_{aq} \quad (12)$$

and for pyrite and magnetite by

$$1/2FeS_2 + 1/3H_{2,aq} + 2/3H_2O_l = 1/6Fe_3O_4 + H_2S_{aq} \quad (13)$$

The results are shown in Figure 15. They suggest that the mineral pair pyrite and pyrrhotite is not in equilibrium with the aquifer water. A possible cause, consistent with the results for pyrite, is that the aquifer water is under-saturated with respect to this mineral. To bring the pair to equilibrium, either H_2 must increase or H_2S decrease, or both. The mineral pair of pyrite and magnetite (Figure 16) is also not in equilibrium, according to the H_2/H_2S ratio. To bring this pair into equilibrium, either H_2 must increase

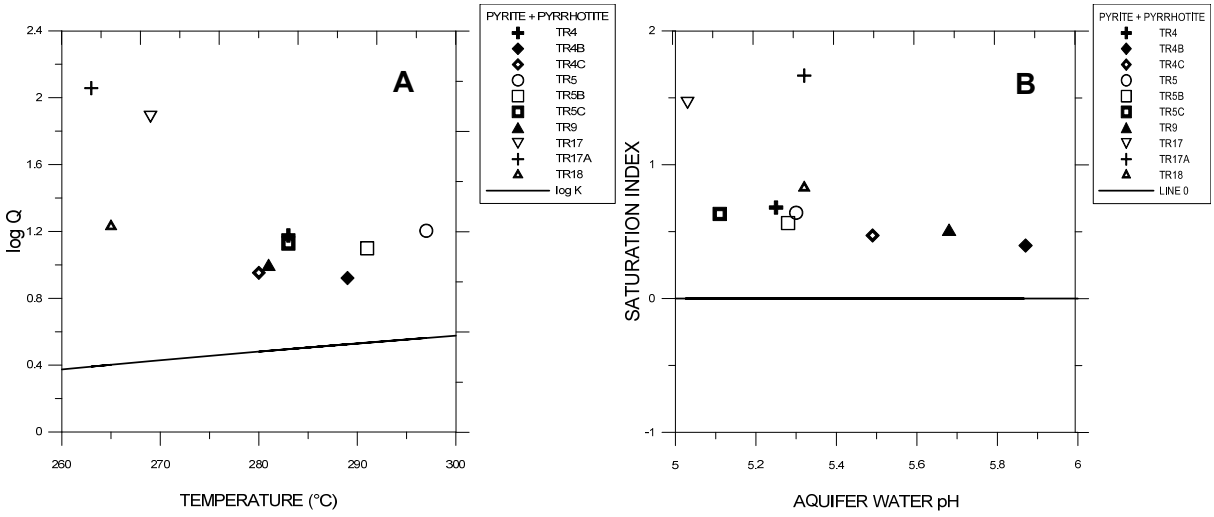

FIGURE 15: a) Log Q and Log K pyrite+pyrrhotite vs. temperature;
b) SI pyrite+pyrrhotite vs. aquifer water pH

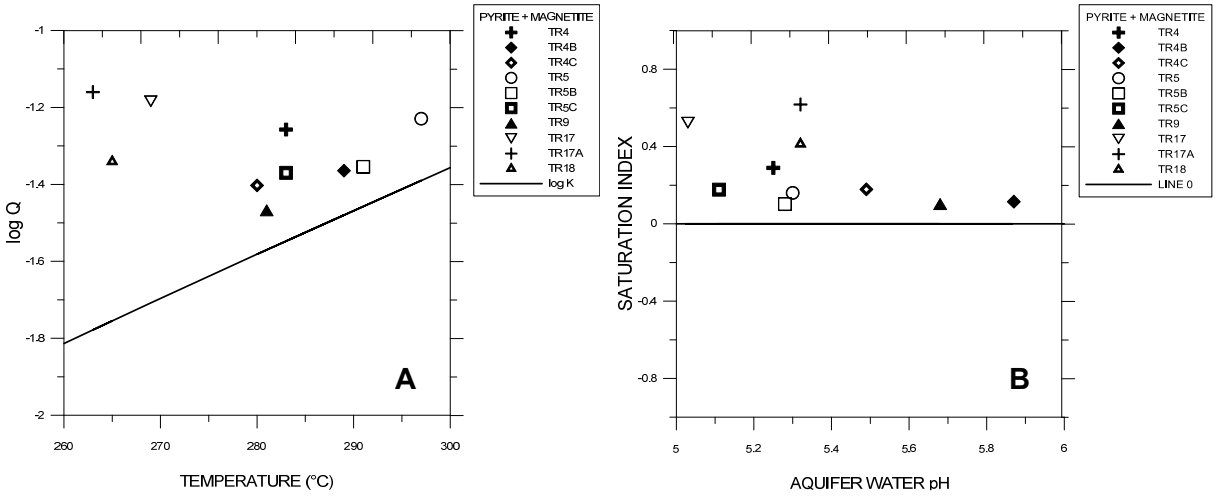

FIGURE 16: a) Log Q and Log K pyrite+magnetite vs. temperature;
b) SI pyrite+magnetite vs. aquifer water pH

or H_2S decrease, just like for the pyrite-pyrrhotite pair. To bring all minerals into equilibrium, it is required to increase H_2 gas concentrations by just under 0.2 on the log scale. This coincidence could be the consequence of a given departure from equilibrium by sulphur species having a valency of -1 and -2, respectively.

To maximize the quality of the modelling of sulphide mineral scaling from the geothermal fluids at Berlín, it is important to have first class analytical data, in particular about pH, iron and other metals forming sulphide minerals and, subsequently, to assess the state of saturation of these minerals in the aquifer water using WATCH. If saturated, boiling of the aquifer water would lead to over-saturation of sulphide minerals and for two reasons. One is that degassing with respect to CO_2 and H_2S leads to an increase in water pH which would reduce sulphide mineral solubility. The other reason is that boiling leads to cooling and sulphide mineral solubilities decrease with decreasing temperatures. The metal concentrations in geothermal fluids, certainly if equilibrium prevails, increase with increasing water salinity. In dilute and relatively dilute geothermal fluids, the metal concentrations are low, but in brines, such as at Salton Sea in California, they are high. Here, the metals forming sulphides are in excess over H_2S on a molal basis but, in dilute and relatively dilute waters, H_2S is in much excess. When this is the case, the amount of sulphide scaling that forms over a given period of time when geothermal waters boil will be controlled by the availability of the sulphide-forming metals. To assess this availability, it may not be sufficient to just analyse metal concentrations in samples collected at the surface. Likely, it will also be necessary to calculate metal-sulphide mineral saturation in the aquifer water, because a large part of the metals may be lost from solution between the aquifer and the wellhead due to their precipitation as sulphides.

8. EFFECTS OF BOILING ON MINERAL SATURATION

The boiling of geothermal water causes changes in its compositions that essentially involve (1) degassing of the water and (2) an increase in its dissolved solids content. Two gases (CO_2 and H_2S) which are invariably major components in geothermal fluids, at least when above about 200°C, form weak acid when dissolved in water. Their removal from the water will cause its pH to increase.

Many minerals, such as calcite, hydroxides and all OH^- bearing silicates, have pH dependent solubility. Increase in the water pH and in the concentrations of dissolved solids upon boiling, as well as cooling, leads to changes in the state of mineral saturation of the water (Arnórsson et al., 2000).

In this study, the effects of boiling on chemical species distribution and, therefore, mineral saturation, emphasizing wells where there is evidence of scale formation, such as well TR5C, where sulphide scales are known to occur, were studied. The WATCH program was used to evaluate the effects of boiling over the whole temperature range down to 100°C. The WATCH program allows activity products for minerals to be calculated and, from this information and the solubility constants for the minerals, their saturation state was evaluated, either depicted as SI (Saturation Index) or as Q values. In the latter case, the equilibrium constant K was plotted on the graphs.

8.1 Calcite and silicate minerals with pH dependent solubility

The aquifer water was calculated to be slightly calcite over-saturated (Figure 17). However, this is not significant and was caused by errors in analytical data and in the thermodynamic data on aqueous species.

When boiling occurs, the temperature of the fluid descends (Figure 17); in view of this, a change in the degassing coefficient is required to evaluate the effects of the degassing of CO_2. When this coefficient is changed in WATCH, the saturation curve declines (see Figure 14b). However, the tendency for increased saturation with a reduction in the temperature is always maintained; this might be due to the fact that degassing is limited at high temperatures and therefore continues to low temperatures. With decreasing temperature Ca-bearing aqueous species may break down and in this way contribute to an increase in aqueous Ca^{+2} activity and at the same time increasing the calcite activity product.

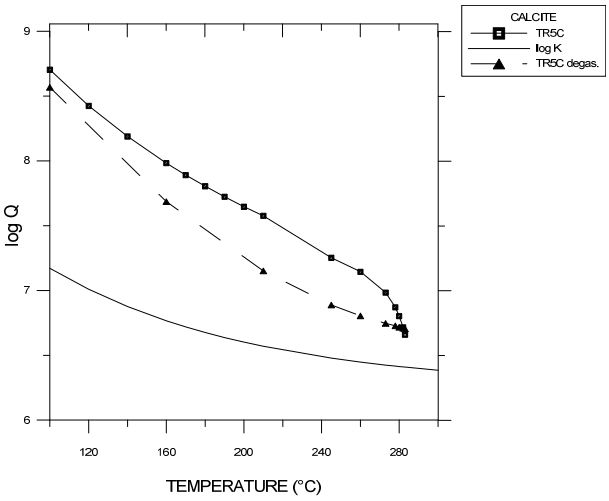

FIGURE 17: Calcite saturation plotted against temperature upon adiabatic boiling. Degassing was assumed to be at maximum (equilibrium degassing, solid line) and 20% of maximum (broken line)

When boiling occurs, the fluid temperature decreases (Figure 17) and this causes an increase in the solubility product (Q) for calcite. During the early stages of boiling, the increase in Q is largely caused by degassing (pH increase) (see Figure 17) but in the late stages of boiling, the extent of degassing has little influence because degassing is practically complete anyway. However, the tendency to increase saturation by boiling (decrease in temperature) is always maintained because the degassing always leads to a substantial increase in CO_3^{-2} activities beyond the increase in calcite solubility with decreasing temperature. The sharp increase in over-saturation during the early stages of boiling indicates that calcite scaling is expected to be most intense at the first depth level of boiling.

Arnórsson (1978) has pointed out that calcite scaling generally only tends to be a problem if boiling starts within the wells. If boiling starts in the producing aquifers, the effect will not be detectable, except possibly in the long run, as the cross section of pore spaces in the aquifer rock are much larger than the cross-sectional area of the wellbore.

Silicate minerals, such as clinozoisite, epidote, and prehnite that have pH dependent solubility, like calcite, also show a tendency for an increase in Q when boiling occurs, followed by a decrease in Q after the water has been practically completely degassed (Figure 18) because the solubility decreases with decreasing temperature of the boiling water. Despite this, these minerals are not expected to form scales because of the slow kinetics of the respective precipitation reactions.

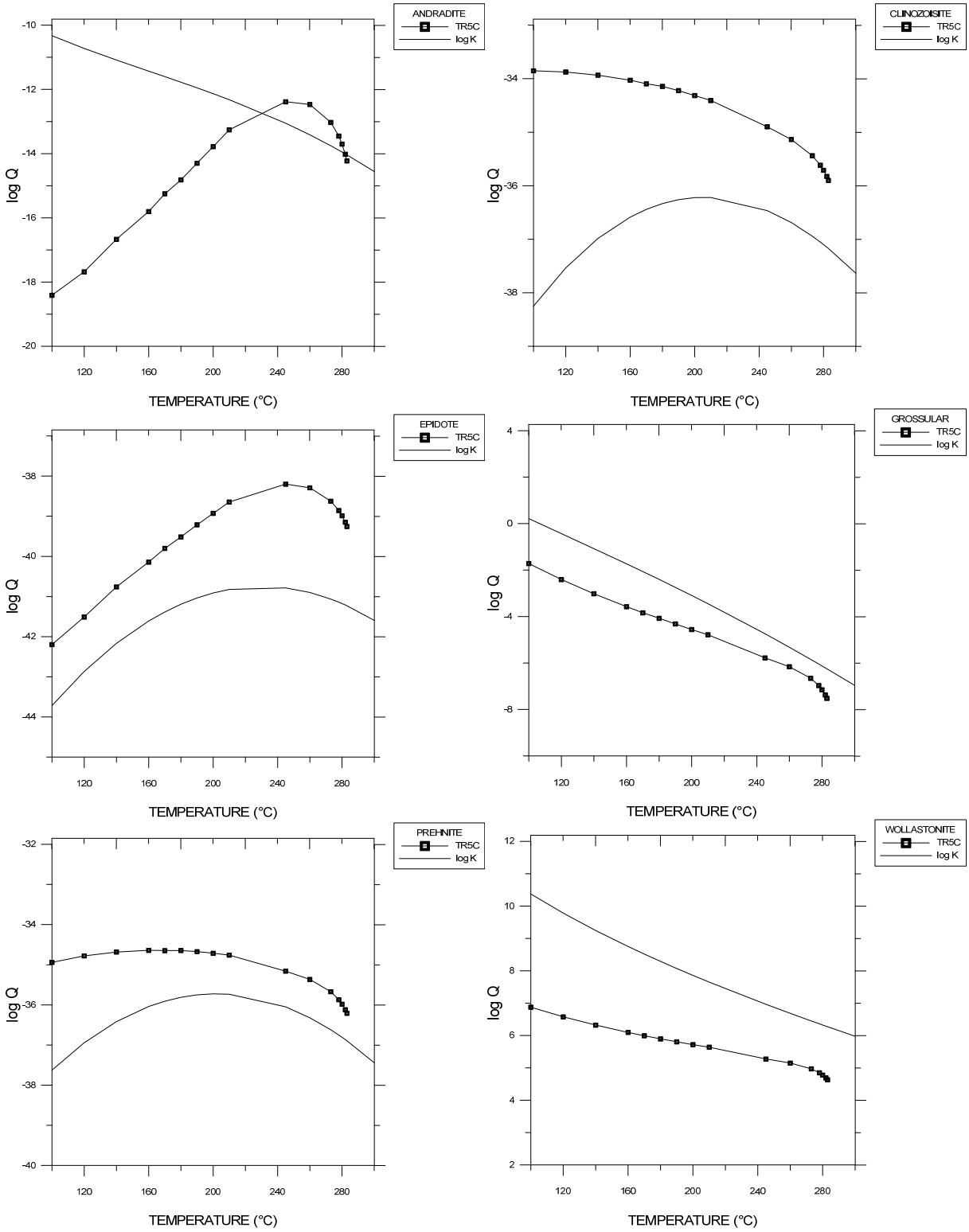

FIGURE 18: Log Q and Log K for andradite, clinozoisite, epidote, grossular, prehnite, and wollastonite vs. temperature

8.2 Pyrite, pyrrhotite and magnetite

In well TR5C, the aquifer water is close to pyrrhotite saturation. Upon boiling of this water, it becomes pyrrhotite over-saturated, due to an increase in pH by H_2S degassing. Pyrrhotite over-saturation

continues to increase as boiling proceeds due to its decreasing solubility with decreasing temperature.

The situation with pyrite is different. The WATCH results indicated that the reservoir water is under-saturated with this mineral. But, upon boiling, the Q value increased strongly, making the water over-saturated. This implies that pyrite should not be present in the deep reservoir and that it forms for the first time where extensive boiling occurs, either in wells or in upflow zones (Figure 19). Researchers studying hydrothermal alteration did not report pyrite (see Tables 2-4). This does not, however, exclude the presence of this mineral. If present, a reasonable explanation for the apparent pyrite under-saturation in the reservoir is the consequence of sulphur-redox disequilibrium. A rigorous test of pyrite saturation would require an analysis of sulphur with a valency of -1 allowing calculation of the activity of the S_2^{-2} species.

Magnetite behaves in a manner very similar to that of pyrite and pyrrhotite (Figure 19). Yet there are some differences that make it resemble calcite more than pyrite and pyrrhotite. An over-saturation is produced during the early stages of boiling followed by an increasing degree of under-saturation. This implies that magnetite could form scales during the early stages of boiling, but it would become unstable during the later stages. Magnetite is not known to form scales from geothermal fluids, except under very special circumstances. Magnetite precipitates from superheated steam (at 120 bar) from the IPPD hole drilled into magma at Krafla in Iceland (Arnórsson, pers. comm.).

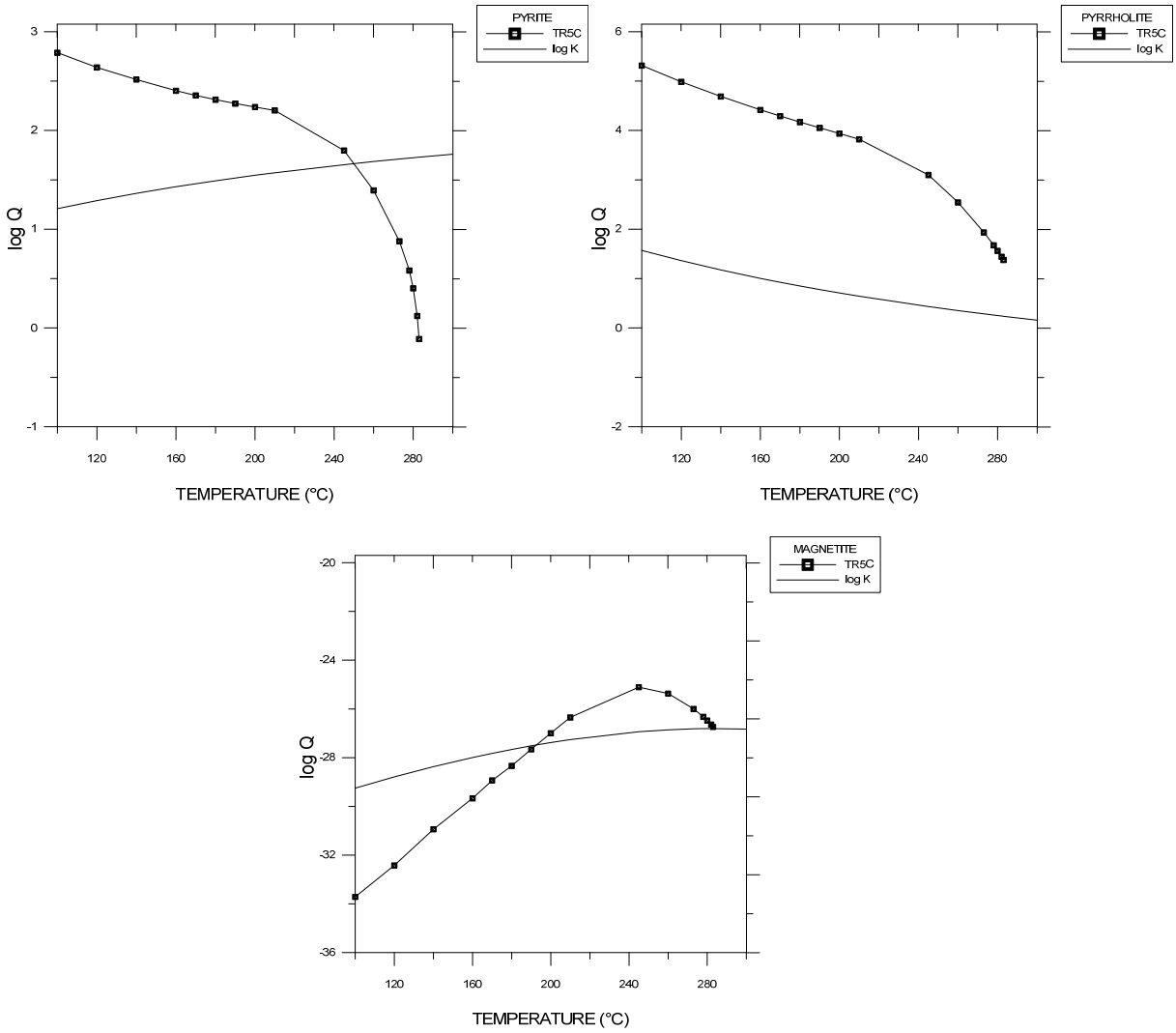

FIGURE 19: Log Q and Log K for pyrite, pyrrhotite, and magnetite vs. temperature

9. SUMMARY AND CONCLUSIONS

At deep levels, the Berlín geothermal reservoir is sub-boiling with temperatures of around 300°C. In some of the producing wells, the first depth level of boiling is within the well but, in other cases, in the feed zone.

The reservoir water is mildly saline and rather homogeneous in composition with 3000-5000 ppm Cl. The reservoir water has closely approached chemical equilibrium with common hydrothermal minerals. Boiling of the reservoir water by depressurization, caused by discharging wells, may lead to mineral precipitation in the formation, in wells and in surface equipment because both degassing of the water and cooling changes mineral activity products and mineral solubility constants. The extent of mineral precipitation, if over-saturation is produced, largely depends on kinetic factors. Thus, silicate minerals are not expected to precipitate, except for amorphous silica and sometimes an amorphous Al-silicate, due to their sluggish kinetics. By contrast, "salts" such as calcite, and metal sulphides have fast kinetics and they can form scales if an initially saturated reservoir water becomes over-saturated upon depressurization boiling.

The rate at which specific minerals form scales depends on several factors: the degree of over-saturation, the kinetic rate constant, the nucleation rate, the surface area between the fluid and minerals once they have nucleated, and the availability of the scale forming chemical components. Thus, in dilute geothermal waters, metals forming sulphide minerals are present in very low concentrations, limiting the amount of scale that forms despite the fast kinetics of sulphide mineral precipitation. The same applies to calcite. In brines, on the other hand, base metals forming sulphides, such as at Salton Sea in California, are abundant and the concentration of H_2S in the brine may be a limiting factor in the amount of sulphide scales that form.

At Berlín, sulphide scales are of concern as they form at substantial rate in some wells. To understand this better, it is considered important to (1) determine all the mineral phases that form the scales, (2) to model the concentrations of sulphide forming metals in the aquifer water by using both analytical data on samples collected at the wellhead and to calculate the concentrations of these metals at equilibrium in the reservoir. The latter approach is considered to be important because a substantial part of these metals may be removed from the water between the aquifer and the wellhead by their precipitation.

ACKNOWLEDGEMENTS

I would like to express my sincere gratitude to the Government of Iceland for granting me the opportunity to attend the UNU-GTP in 2012, and to the UNU Geothermal Training Programme staff, Director, Dr. Ingvar Birgir Fridleifsson, Deputy Director, Mr. Lúdvík S. Georgsson, Ms. Málfrídur Ómarsdóttir, Ms. Thórhildur Ísberg, Mr. Ingimar G. Haraldsson and Mr. Markús A.G. Wilde, for their support throughout this training. I am also deeply grateful to my supervisor, Dr. Stefan Arnórsson for his patience, dedication, help, guidance and advice during the project.

I would like to extend my gratitude to my employer, LaGeo S.A. de C.V., for giving me the opportunity to participate in this programme.

My deepest thanks go to my parents, Francisco Abel and Zoila Elba de Hernandez, for their prayers, guidance and encouragement all my life. I give all my love to the Holy Family: God, Maria and Jesus Christ, who have been with me all the time, in my mind and heart.

Finally, I am very grateful to all the 2012 UNU Fellows, for wonderful moments we shared during this period; it was a real pleasure to meet with each and everyone of you.

REFERENCES

Arnórsson, S., 1978: Precipitation of calcite from flashed geothermal waters in Iceland. *Contrib. Mineral. Petrol., 66,* 21-28.

Arnórsson, S., 1991: Geochemistry and geothermal resources in Iceland, In: D´Amore, F. (co-ordinator), *Applications of geochemistry in geothermal reservoir development.* UNITAR/UNDP publication, Rome, 145-196.

Arnórsson, S., 1999: The relative abundance of Al-species in natural waters in Iceland. *Proceedings of the 5th International Symposium on the Geochemistry of the Earth´s Surface, Balkema, Rotterdam,* 421-424.

Arnórsson, S., D´Amore, F. and Gerardo-Abaya, J., 2000: *Isotopic and chemical techniques in geothermal exploration, development and use. Sampling methods, data handling, interpretation*. International Atomic Energy Agency, Vienna, 351 pp.

Arnórsson, S., and Andrésdóttir, A., 1999: The dissociation constants of Al-hydroxy complexes at 0-350°C and P_{sat}. *Proceedings of 5th International Symposium on the Geochemistry of the Earth´s Surface*, *Rotterdam, Balkema,* 425-428.

Arnórsson, S., Gunnarsson, I., Stefánsson, A., Andrésdóttir, A., and Sveinbjörnsdóttir, Á.E., 2002: Major element chemistry of surface- and ground waters in basaltic terrain, N-Iceland.: I. Primary mineral saturation. *Geochim. Cosmochim. Acta, 66,* 4015-4046.

Arnórsson, S., Sigurdsson, S., and Svavarsson, H., 1982: The chemistry of geothermal waters in Iceland I. Calculation of aqueous speciation from 0°C to 370°C. *Geochim. Cosmochim. Acta, 46,* 1513-1532.

Bjarnason, J.Ö., 1994: *The speciation program WATCH, version 2.1.* Orkustofnun, Reykjavík, 7 pp.

CEL, 1999: *Final drilling report of directional well TR-1A, Berlín geothermal field, El Salvador.* CEL, División de Generación Geotérmica, Santa Tecla, El Salvador, internal report (in Spanish).

Diakonov, I.I., Schott, J., Martin, F., Harrichourry, J.C., and Escalier, J., 1999: Iron (III) solubility and speciation in aqueous solutions. Experimental study and modelling: part 1. Hematite solubility from 60 to 300 °C in NaOH–NaCl solutions and thermodynamic properties of Fe(OH)4,aq. *Geochim. Cosmochim. Acta, 63*, 2247–2261.

Electroconsult, 1993: *Berlín geothermal field*. CEL, Santa Tecla, report of geoscientific investigations (in Spanish).

Fernandez-Prini, R., Alvarez, J.L., and Harvey, A.H., 2003: Henry´s constants and vapour liquid distribution constants for gaseous solutes in H_2O and D_2O at high temperatures. *J. Phys. Chem. Ref. Data, 32*, 903-916.

Fournier, R.O., and Potter, R.W. II, 1982a: A revised and expanded silica (quartz) geothermometer. *Geoth. Res. Council Bull., 11-10*, 3-12.

Fournier, R.O., and Potter, R.W. II, 1982b: An equation correlating the solubility of quartz in water from 25° to 900°C, at pressures up to 10,000 bars. *Geochim. Cosmochim Acta, 46*, 1969-1973.

Fournier, R.O., and Rowe, J.J., 1966: Estimation of underground temperatures from the silica contents of water from hot springs and wet steam wells. *Am. J. Sci., 264,* 685-697.

Gunnarsson, I., and Arnórsson, S., 2000: Amorphous silica solubility and the thermodynamic properties of $H_4SiO_4°$ in the range of 0° to 350°C at P_{sat}. *Geochim. Cosmochim. Acta, 64*, 2295-2307.

Helgeson, H.C., 1967: Thermodynamics of complex dissociation in aqueous solution at elevated temperatures. *J. Phys. Chem., 71*, 3121-3136.

Hernandez M., C.B., 2012: *Appendix II to the report "Aquifer fluid compositions at the Berlín geothermal field, El Salvador in 2012"*. UNU-GTP, Iceland, report 12, appendix II, 12 pp.

Holland, T.J.B., and Powell, R., 1998: An internally consistent thermodynamic data set for phases of petrological interest. *J. Metamorph. Geol., 16*, 309-343.

Johnson, J.W., Oelkers, E.H., and Helgeson, H.C., 1992: SUPCRT92: A software package for calculating the standard molar properties of minerals, gases, aqueous species and reactions among them from 1 to 5000 bar and 0 to 1000°C. *Comp. Geosci., 18*, 899-947

Karingithi, C.W., Arnórsson, S., and Grönvold, K., 2010: Processes controlling aquifer fluid compositions in the Olkaria geothermal system, Kenya. *J. Volcanology & Geothermal Research, 196,* 57-76.

Melara E., E.E., 2011: Calcite scaling in geothermal production wells in El Salvador, current situation and control methodology. Report 23 in: *Geothermal Training in Iceland 2011*. UNU-GTP, Iceland, 513-544.

Molnar, P., and Sykes, L.R., 1969: Tectonics of the Caribbean and Middle America regions from focal mechanisms and seismicity. *Geological Society of America Bulletin, 80*, 1639-1684.

Montalvo, F., and Axelsson, G., 2000: Assessment of chemical and physical reservoir parameters during six years of production-reinjection at Berlín geothermal field (El Salvador). *Proceedings of the World Geothermal Congress 2000, Kyushu-Tohoku, Japan*, 2153-2158.

Nordstrom, D.K., and Jenne, E.A., 1977: Fluorite solubility equilibria in selected geothermal waters. *Geochim. Cosmochim. Acta, 41*, 175-188.

Plummer, L.N., and Busenberg, E., 1982: The solubilities of calcite, aragonite and vaterite in CO_2-H_2O solutions between 0 and 90°C, and evaluation of the aqueous model for the system $CaCO_3$-CO_2-H_2O. *Geochim. Cosmochim. Acta, 46*, 1011-1040.

Pokrovskii, V.A., and Helgeson, H.C., 1995: Thermodynamic properties of aqueous species and solubilities of minerals at high pressures and temperatures: the system Al_2O_3–H_2O–NaCl. *Amer. J. Sci., 295*, 1255-1342.

Robie, R.A., and Hemingway, B.S., 1995: *Thermodynamic properties of minerals and related substances at 298.15 K and 1 bar (105 Pascals) pressures and at higher temperatures.* USGS Bull., 2131, 461 pp.

Rodriguez, V.A., and Monterrosa, M.E., 2011: Field monitoring and management: The Berlín geothermal field case (presentation slides). *Presented at the "Short Course on Geothermal Drilling, Resource Development and Power Plants", organized by UNU-GTP and LaGeo, in Santa Tecla, El Salvador*.

Santos, P.A., 1995: One and two-dimensional interpretation of DC-resistivity data from the Berlín geothermal field, El Salvador. Report 11 in: *Geothermal Training in Iceland 1995*. UNU-GTP, Iceland, 269-302.

APPENDIX I: Temperature and pressure loggings from the 11 wells evaluated

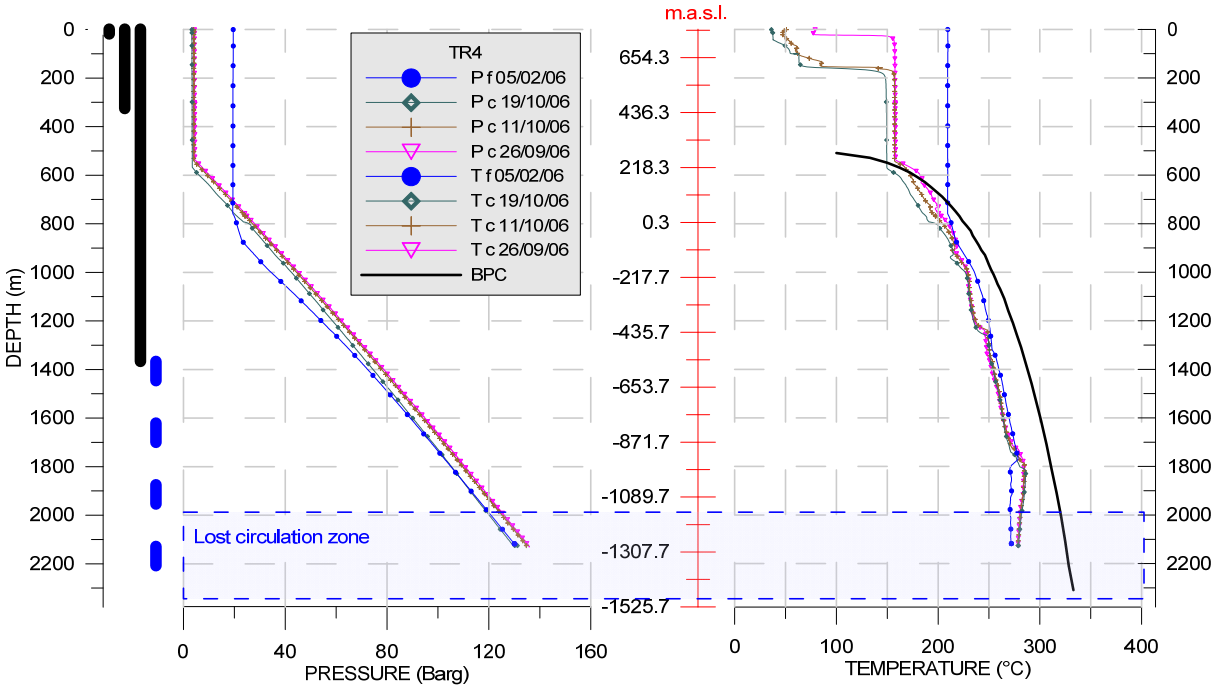

FIGURE 1: Temperature and pressure run in well TR4; P and T denote pressure and temperature, respectively; subscripts have the following notations: c= well closed, f= well discharging. BPC is the boiling point curve with depth calculated from the water rest level, assuming the water in the well to be at the boiling point at all depths.

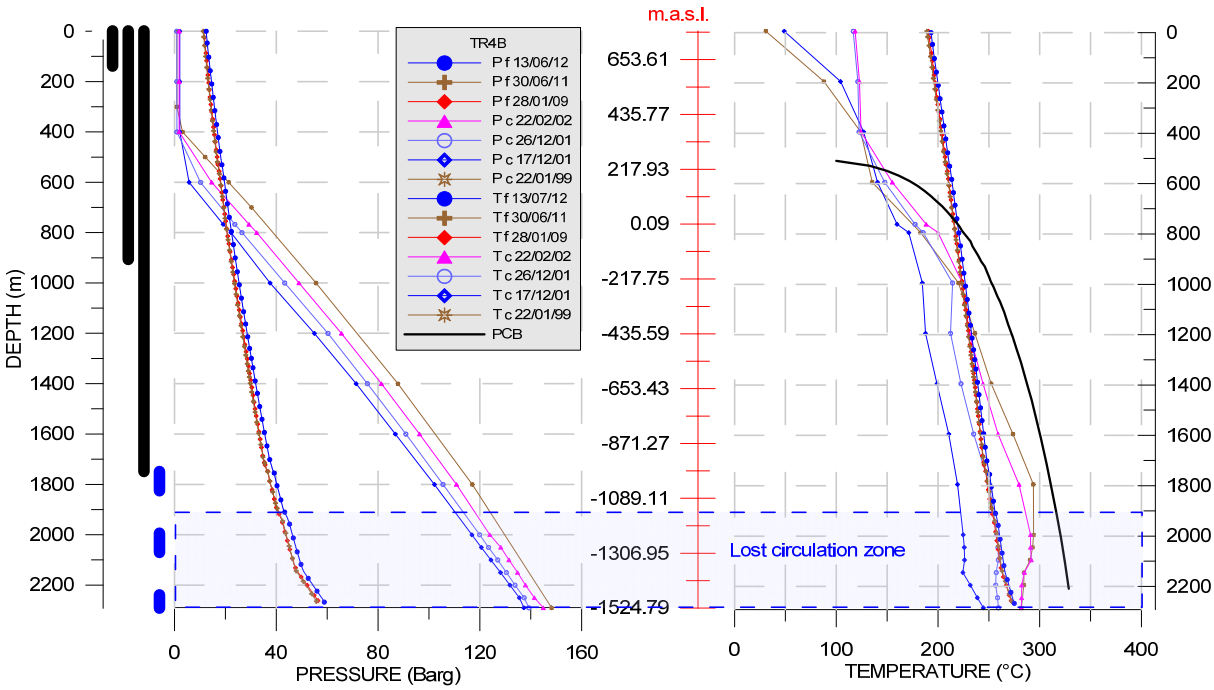

FIGURE 2: Temperature and pressure run in well TR4B; See Figure 1 for legends

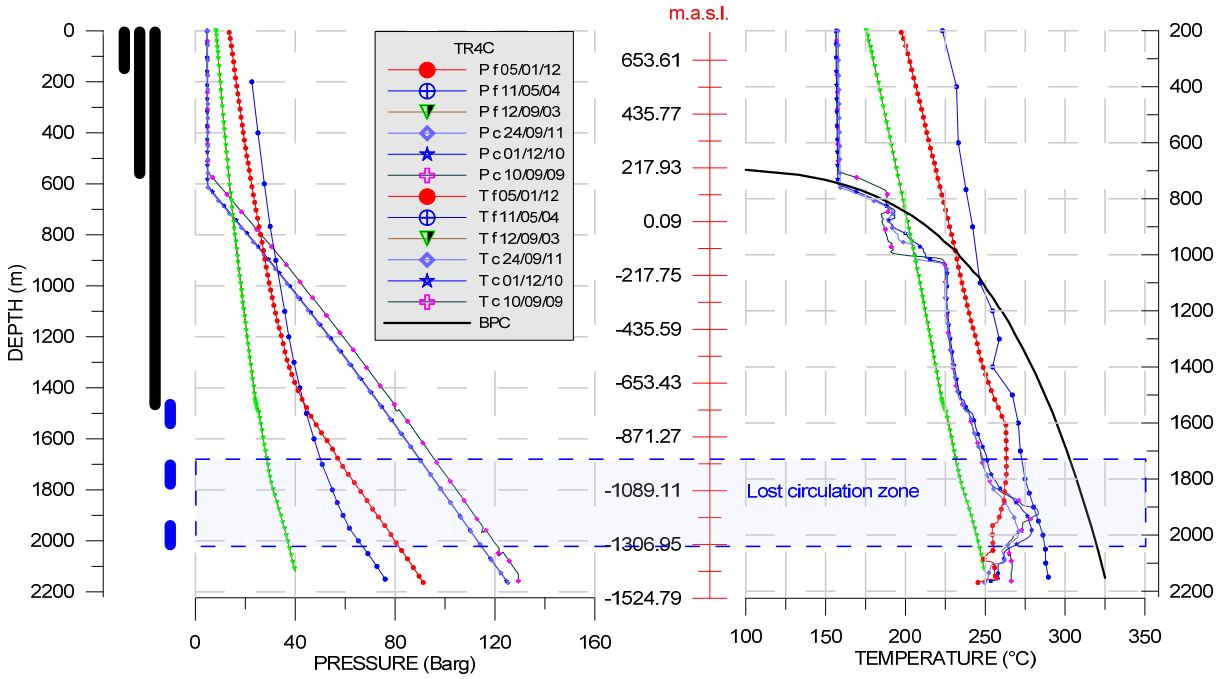

FIGURE 3: Temperature and pressure run in well TR4C; See Figure 1 for legends

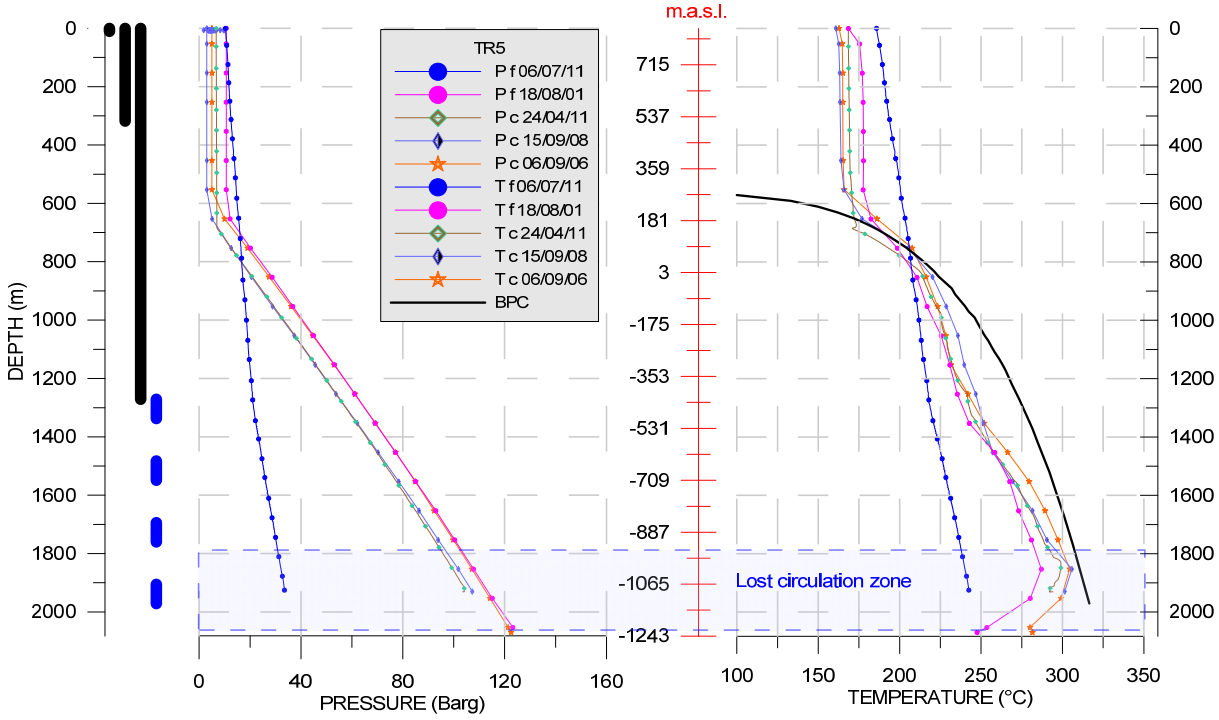

FIGURE 4: Temperature and pressure run in well TR5; See Figure 1 for legends

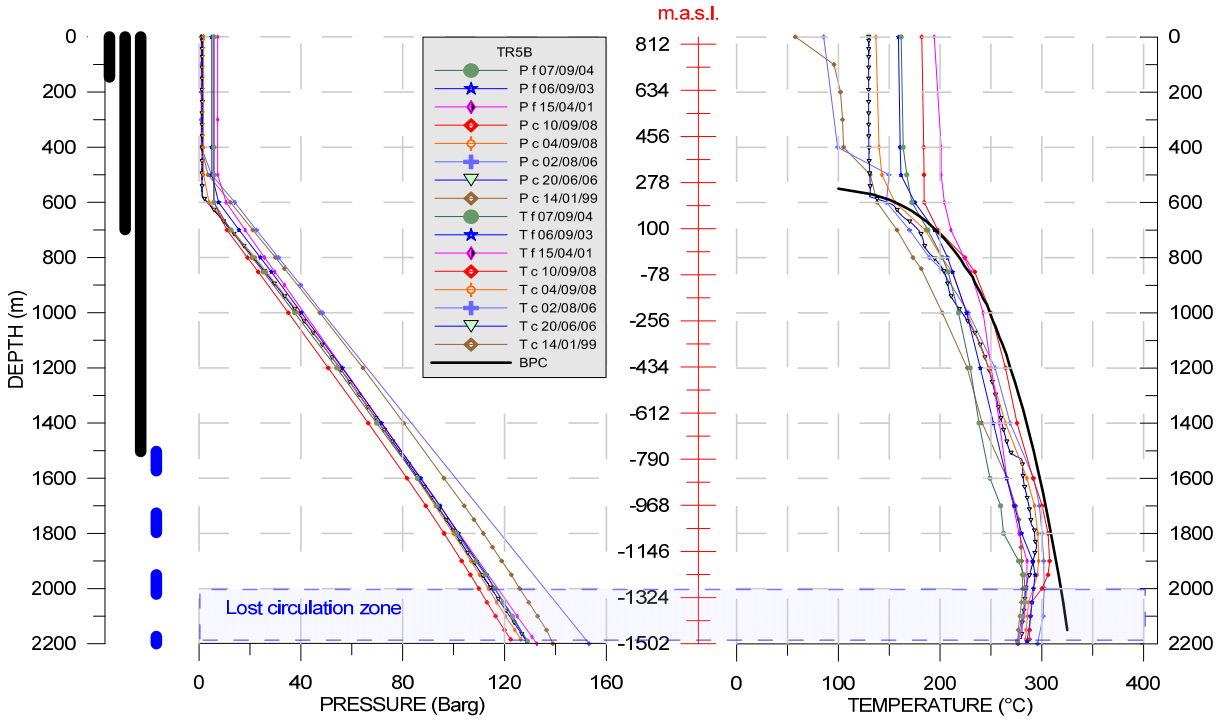

FIGURE 5: Temperature and pressure run in well TR5B; See Figure 1 for legends

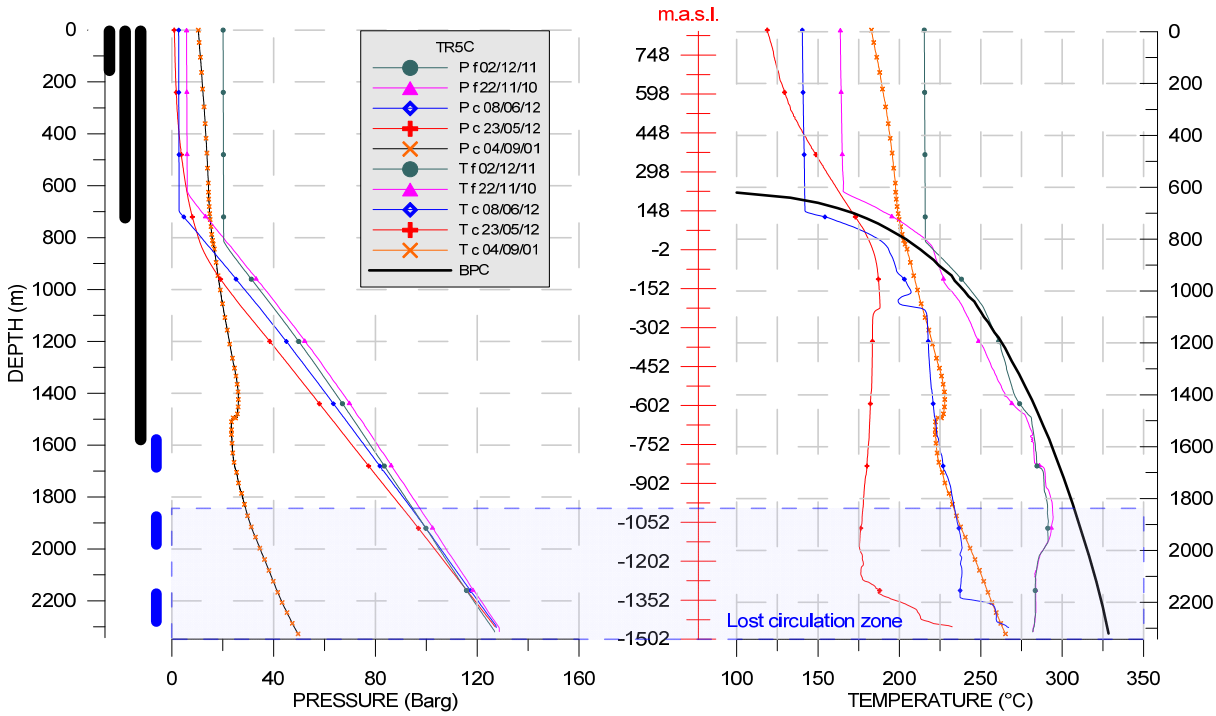

FIGURE 6: Temperature and pressure run in well TR5C; See Figure 1 for legends

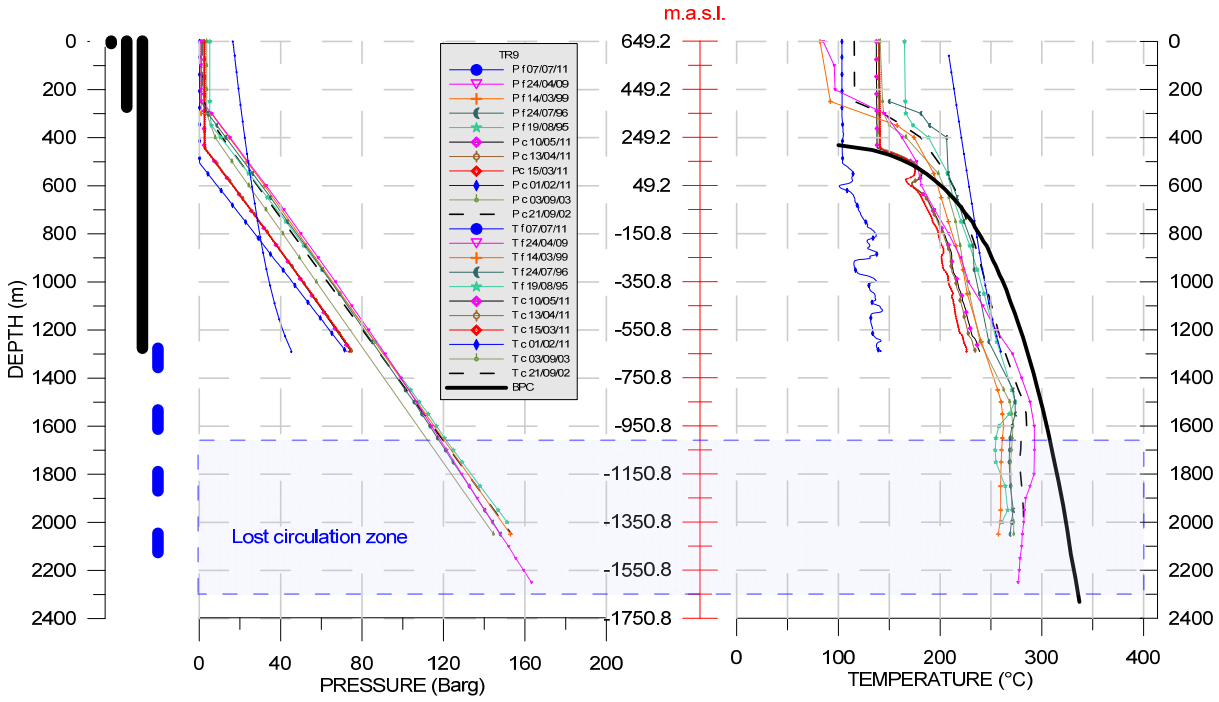

FIGURE 7: Temperature and pressure run in well TR9; See Figure 1 for legends

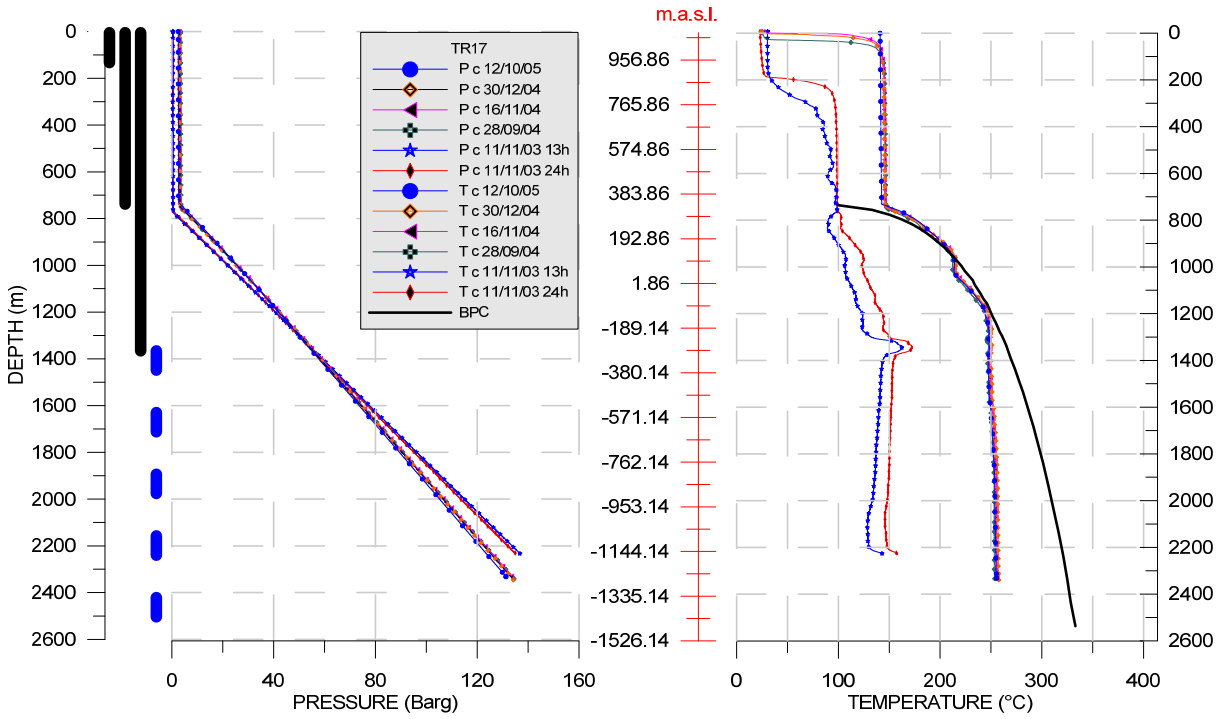

FIGURE 8: Temperature and pressure run in well TR17; See Figure 1 for legends

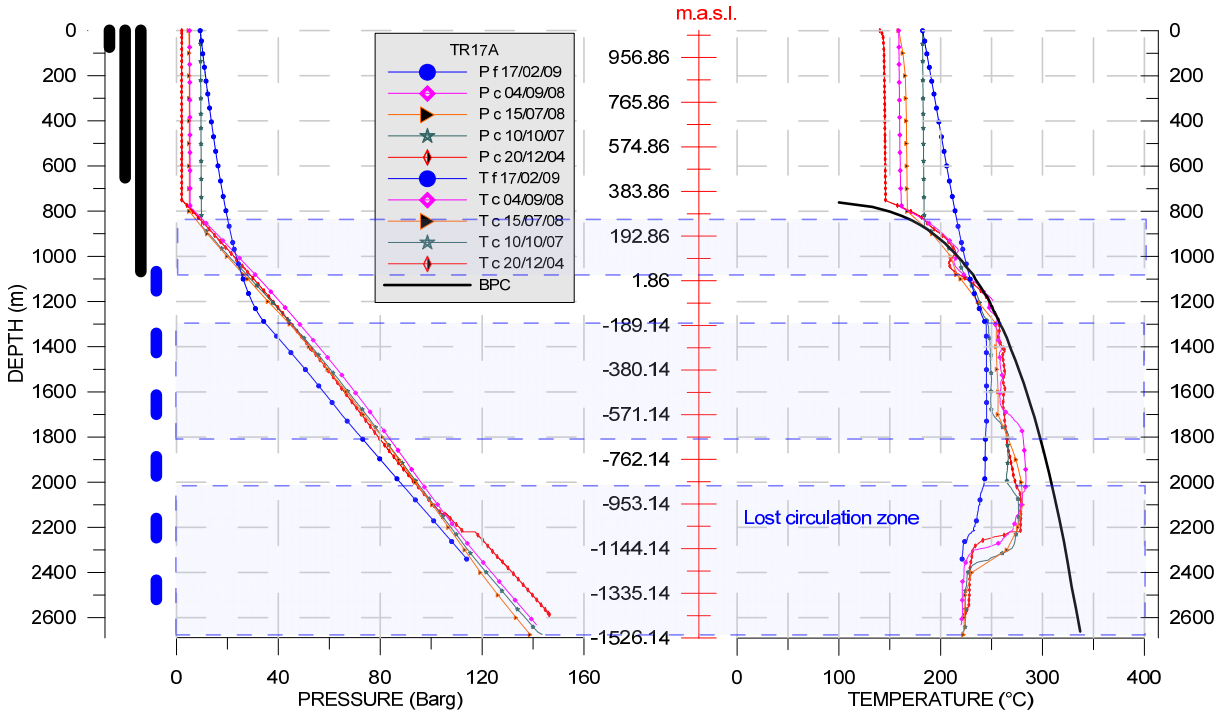

FIGURE 9: Temperature and pressure run in well TR17A; See Figure 1 for legends

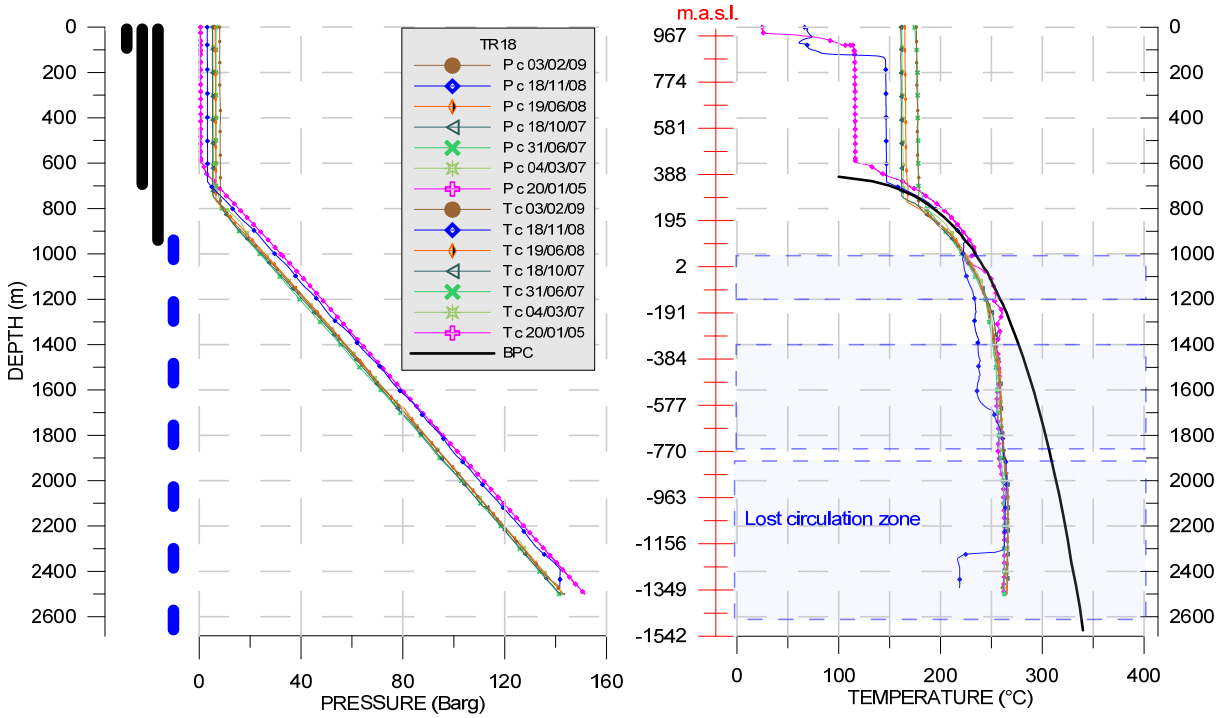

FIGURE 10: Temperature and pressure run in well TR18; See Figure 1 for legends

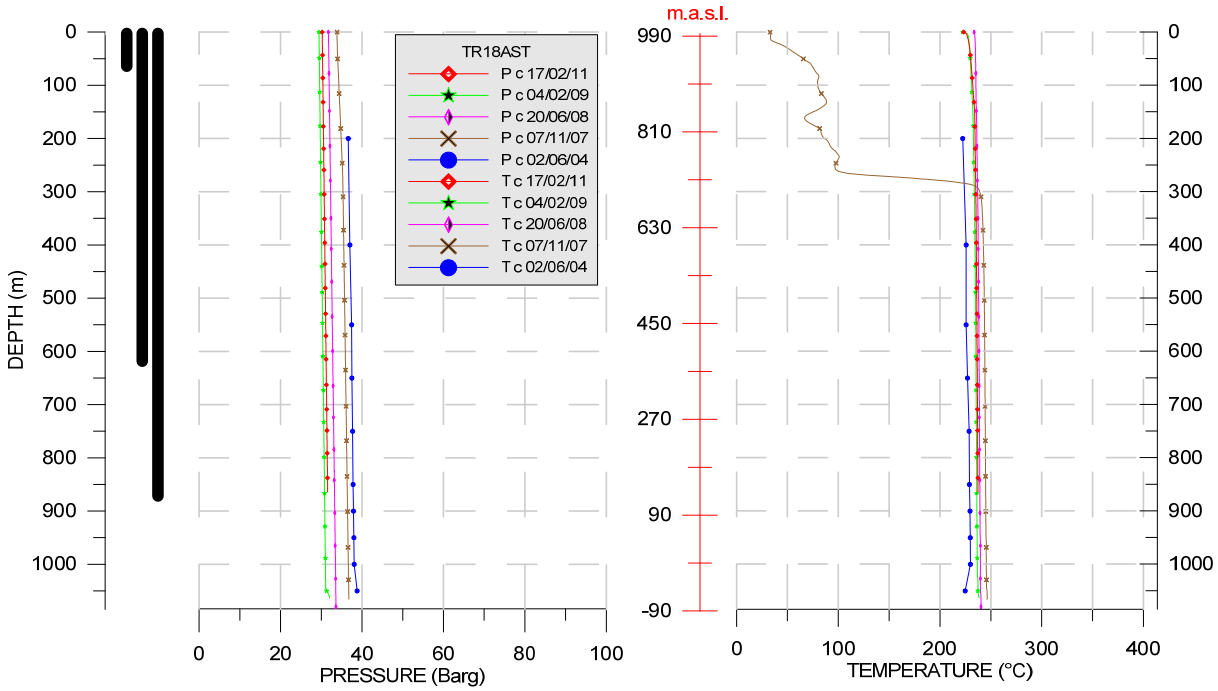

FIGURE 11: Temperature and pressure run in well TR18A; See Figure 1 for legends